NASA TECHNICAL MEMORANDUM

NASA TM X-2030

NASA TM X-2030



# EXPERIMENTAL STUDY OF GROOVE PATTERNS ON ABLATED SURFACES IN THE LANGLEY 8-FOOT HIGH-TEMPERATURE STRUCTURES TUNNEL

*by L. Roane Hunt and W. E. Bruce, Jr.*

*Langley Research Center*
*Hampton, Va.* 23365

NATIONAL AERONAUTICS AND SPACE ADMINISTRATION • WASHINGTON, D. C. • JUNE 1970

| 1. Report No. | 2. Government Accession No. | 3. Recipient's Catalog No. |
|---|---|---|
| NASA TM X-2030 | | |

| 4. Title and Subtitle | 5. Report Date |
|---|---|
| EXPERIMENTAL STUDY OF GROOVE PATTERNS ON ABLATED SURFACES IN THE LANGLEY 8-FOOT HIGH-TEMPERATURE STRUCTURES TUNNEL | June 1970 |
| | 6. Performing Organization Code |

| 7. Author(s) | 8. Performing Organization Report No. |
|---|---|
| L. Roane Hunt and W. E. Bruce, Jr. | L-6979 |
| | 10. Work Unit No. 126-63-11-33 |
| 9. Performing Organization Name and Address<br>NASA Langley Research Center<br>Hampton, Va. 23365 | 11. Contract or Grant No. |
| | 13. Type of Report and Period Covered<br>Technical Memorandum |
| 12. Sponsoring Agency Name and Address<br>National Aeronautics and Space Administration<br>Washington, D.C. 20546 | 14. Sponsoring Agency Code |

15. Supplementary Notes

16. Abstract

An investigation was made in the Langley 8-foot high-temperature structures tunnel to study the formation of ablation patterns on teflon surfaces of large cone and wedge models and on wood and Lexan surfaces of wedge models immersed in a high-enthalpy hypersonic stream. The tests were conducted at a Mach number of 7.4, at total temperatures between 1810 K and 1970 K, and at stream unit Reynolds numbers between $0.35 \times 10^6$ and $0.55 \times 10^6$ per meter. The results indicate that a turbulent boundary layer is necessary for the formation of groove patterns and that the local Mach number affects the groove angle. Also, a rearward-facing step in the turbulent boundary layer appears to cause the pattern to be more extensive. The patterns have a characteristic groove spacing, and they do not propagate laterally.

| 17. Key Words (Suggested by Author(s)) | 18. Distribution Statement |
|---|---|
| Groove patterns<br>Ablation | Unclassified – Unlimited |

| 19. Security Classif. (of this report) | 20. Security Classif. (of this page) | 21. No. of Pages | 22. Price* |
|---|---|---|---|
| Unclassified | Unclassified | 57 | $3.00 |

*For sale by the Clearinghouse for Federal Scientific and Technical Information
Springfield, Virginia 22151

# EXPERIMENTAL STUDY OF GROOVE PATTERNS ON ABLATED SURFACES IN THE LANGLEY 8-FOOT HIGH-TEMPERATURE STRUCTURES TUNNEL

By L. Roane Hunt and W. E. Bruce, Jr.
Langley Research Center

## SUMMARY

An investigation was made in the Langley 8-foot high-temperature structures tunnel to study the formation of ablation patterns on teflon surfaces of large cone and wedge models and on wood and Lexan surfaces of wedge models immersed in a high-enthalpy hypersonic stream. The tests were conducted at a Mach number of 7.4, at total temperatures between 1810 K and 1970 K, and at stream unit Reynolds numbers between $0.35 \times 10^6$ and $0.55 \times 10^6$ per meter. The results indicate that a turbulent boundary layer is necessary for the formation of groove patterns and that the local Mach number affects the groove angle. Also, a rearward-facing step in turbulent flow appears to cause the pattern to be more extensive. The patterns have a characteristic groove spacing, and they do not propagate laterally.

## INTRODUCTION

Orderly diamond-shaped groove patterns on ablated surfaces have been observed in ground tests and on recovered flight vehicles. The cause and propagation of the patterns are not fully understood. Since the surface features of recovered flight vehicles are the result of a time-integrated ablation process, definitive conclusions regarding the mechanics of the process are difficult to infer from the appearance of the final pattern. As a consequence, controlled laboratory test programs are required to determine the cause and characteristics of the patterns.

Previous experimental studies of this groove phenomenon have included ballistics range tests (refs. 1 and 2) and wind-tunnel tests (refs. 3, 4, and 5) conducted in relatively low-enthalpy environments. In these studies, the ablation materials were low-temperature melting ablators, which differed markedly from the ablators used in flight application. To simulate the flight condition of model size and surface material more realistically, a ground test program with higher enthalpy environments, large models, and subliming ablators was conducted. (See refs. 6 and 7.)

The present tests, which were part of the ground test program, were made in the Langley 8-foot high-temperature structures tunnel. The tests were conducted at a Mach number of 7.4, at total temperatures between 1810 K and 1970 K, at stream enthalpies between 2.34 and 2.55 MJ/kg, and at stream unit Reynolds numbers between $0.35 \times 10^6$ and $0.55 \times 10^6$ per meter. The primary test material was teflon, which was tested on the surfaces of large cone and wedge models. Wedge models of Lexan and wood were also tested. Some models were tested with prefabricated flow disturbances, such as holes and protuberances, installed on the model surface. The test results are presented as photographs and tracings of the groove patterns on the model surfaces. Heat-transfer and pressure data obtained during the test program are also presented. Limited results from these tests have been previously reported in references 6 and 7.

## SYMBOLS

The units used for the physical quantities in this paper are given in the International System of Units (SI) as set forth in reference 8.

| | |
|---|---|
| d | cone base diameter, cm |
| $l$ | model wetted length along surface from nose tip or leading-edge apex, cm (see figs. 1, 4, and 6) |
| M | Mach number |
| $N_{Pr}$ | Prandtl number |
| $N_{Re}$ | Reynolds number, based on length $l$ |
| $N_{St}$ | Stanton number |
| p | pressure, $N/m^2$ |
| T | temperature, K |
| t | test duration, s |
| w | transverse distance along wedge surface from center line, cm (see fig. 4) |
| y | normal height above model surface, cm |

$\alpha$ angle of attack, deg

$\delta_T$ turbulent-boundary-layer thickness, cm

$\phi$ angular location around cone model, deg (see fig. 1)

$\theta$ groove angle, deg (see fig. 23)

Subscripts:

1 tunnel free-stream static

2 local static

3 local pitot

t total

Superscripts:

* reference temperature (ref. 9)

' defined within disturbance area (see fig. 11(a))

## MODELS AND TESTS

### Models

Calibration cone.- A calibration cone with a semivertex angle of 36° was tested to determine heat-transfer rate and pressures on a nonablative cone surface in the Langley 8-foot high-temperature structures tunnel. The aluminum model had a smooth stainless-steel nose tip and was instrumented with 24 slug calorimeters and 10 surface pressure orifices. (See ref. 10 for details.) The calorimeters were copper masses of 0.9 gram each and were mounted flush with the model surface along two flow meridians 180° apart. Also, four boundary-layer rakes were attached to the base of the cone to measure pitot pressures circumferentially and radially. A sketch and a photograph of the calibration cone are presented as figures 1 and 2, respectively. A photograph of a set of boundary-layer rakes is presented as figure 3. The longitudinal and angular positions of the calorimeters and pressure orifices are listed in table I(a), and the boundary-layer-probe heights above the cone surface and angular positions are listed in table I(b).

Wedges.- Five wedge configurations, designated W-0 to W-4, with semivertex angles of $30^{o}$ were tested. A sketch of a wedge is presented as figure 4. Each model was a wedge structure with an ablative panel 1.26 cm thick mounted on each side and with a sharp leading edge of solid stainless steel. The four zones (designated zones I, II, III, and IV) defined in figure 4 were used to identify the test areas of the wedge configurations.

Panels of wood, Lexan, and teflon were tested. Photographs of typical panels are presented as figure 5. The wood panel shown in figure 5(a) consisted of successive boards of oak, maple, and pine. The wood grain was transverse to the flow. Lexan, which is a melting ablator, was tested on two wedge configurations. One of the configurations (fig. 5(b)) had a Lexan panel on each side of the wedge. On the other configuration (fig. 5(c)), a Lexan panel was placed adjacent to a teflon panel on one side only. Teflon was tested on four of the wedge configurations.

Thermocouple-instrumented insert plates were mounted on wedge configurations W-4 and W-2 and are shown in figures 5(c) and 5(d). The insert plates were used to determine surface heat flux and were made from AISI C1018 steel 5.1 mm thick. The thermocouples were welded to the back sides of the plates at the positions given in table II.

Teflon cones.- Seven teflon cones, designated C-1 to C-7, were tested. A sketch of a cone and a photograph of a typical tunnel installation are presented as figures 6 and 7, respectively. Each model consisted of a teflon shell 1.26 cm thick installed over the calibration cone structure and a properly sized nose tip to hold the shell in place.

Boundary-layer trips.- Boundary-layer trips were fabricated on some of the nose tips to promote a turbulent boundary layer over the model surface. A sketch is presented in figure 8 to show the location and size of the double raised strip, double grooved strip, and the distributed-roughness trips used on the leading edge of the wedge. A sketch and a photograph to show the various types of boundary-layer trips used on the ablative cone models are presented as figures 9 and 10, respectively.

Ablative-surface flow disturbances.- Prefabricated flow disturbances consisting of holes and protruding pins of various sizes and arrangements were fabricated on the ablative surfaces of two teflon wedges and two cones (W-3, W-4, C-5, and C-6). Sketches showing the location of the distrubances on developed surfaces of the wedges and cones are presented as figures 11 and 12, respectively. Descriptions of the individual disturbances are given in table III.

## Tests

The tests were conducted in the Langley 8-foot high-temperature structures tunnel, which is a large blowdown wind tunnel that uses methane-air combustion to obtain a high

total energy level, and the resulting combustion products are used as the test medium. The thermodynamic, transport, and flow properties of the test medium are given in reference 11. Models were sting mounted from a hydraulically actuated elevator carriage. After the desired flow conditions were established in the tunnel, the model was inserted into the test stream for the duration of the test. The insertion and retraction times were approximately 1 second.

The tunnel total temperature and pressure, the test duration, the model angle of attack, the type of nose tip, and the type of material tested are listed in table IV. The table values of temperature and pressure were recorded at the midpoint of the test duration and are considered to be representative of the entire test duration. The models were tested at an angle of attack of $0^{\circ}$ with exception of the teflon cone C-4 and the Lexan wedge W-1 which were tested at an angle of attack of $4^{\circ}$.

## RESULTS AND DISCUSSION

### Calibration Results

Heating distributions.- The aerodynamic heating distributions along the surface of the calibration cone and along the insert plates of the wedge models are presented in the form of Stanton numbers as figures 13 and 14. The Stanton number is plotted against the local Reynolds number, which is based on model length $l$. The parameters were computed by using Eckert's reference-temperature method (ref. 9) and are compared with laminar and turbulent boundary-layer theory (ref. 12).

The heating results for the $36^{\circ}$ calibration cone (fig. 13) were obtained from calorimeter temperature-time histories for the first 3 seconds of testing. An inverse solution was used to obtain heat-transfer coefficients corrected for the effect of the heat loss from the slug calorimeter to the model wall. The results indicate that for the cone with a smooth nose tip, transition from a laminar boundary layer to a turbulent boundary layer occurred at $N^{*}_{Re} = 1.45 \times 10^{6}$, which corresponds to a length of 21.6 cm. As may be observed, the laminar and turbulent heating levels were adequately predicted by theory.

The aerodynamic heating distribution along the surface of the insert plate of a $30^{\circ}$ wedge (fig. 14) was computed from thermocouple temperature-time histories by using the thin-wall heat-transfer techniques. The data were obtained from tests made with boundary-layer trips on the leading edge, and the comparison of the results with theory indicates that the boundary layer was turbulent over the insert plate.

Pressure distributions.- The circumferential pressure distributions at two longitudinal locations on the $36^{\circ}$ cone are presented in figure 15. The ratio of the measured surface pressure to the computed value of free-stream pressure is plotted against circumferential location on the cone. The different pressure levels indicated for the forward

and aft locations are believed to reflect a variation in free-stream static pressure. Surveys across the diameter of the stream have indicated free-stream static-pressure variations which may reasonably account for the 10-percent pressure difference shown. Complete tunnel surveys have not been documented.

The pitot-pressure distribution normal to the surface of a $36^{\circ}$ cone is presented in figure 16. The ratio of the pitot pressure at $l/d = 0.843$ to the surface pressure of the cone at $l/d = 0.714$ is plotted against the ratio of normal probe height to the theoretical turbulent-boundary-layer thickness. The boundary-layer transition location indicated by the heating results was used in the boundary-layer thickness computation. The experimental data do not indicate the pressure distribution within the boundary layer; however, the level of $p_{t,3}/p_2$ outside the boundary layer is well predicted by the inviscid-flow theory for a $36^{\circ}$ cone. Although the surface-pressure variation along the cone is significant, the ratio of the measured values of pitot pressure to surface pressure is believed to be a good indication of the local Mach number. The inviscid-flow theory was used to compute the Mach number at the edge of the boundary layer for each test condition. The local Mach numbers for the cones and wedges were 2.37 and 2.50, respectively, and the Mach numbers for the windward and leeward sides of the cone at an angle of attack of $4^{\circ}$ were 2.06 and 2.70, respectively.

## Groove Patterns on Various Ablated Surfaces

During the testing, the test surfaces received random impacts by foreign particles that originated from inaccessible upstream areas of the tunnel and hence were not removed by the normal cleaning procedures. These small impacts, which diminished in number and size as the testing progressed, caused local flow disturbances which resulted in attendant grooving of the teflon surface. These local grooves were easily identified, however, and did not influence the onset and extent of the overall aerodynamic grooving pattern. The particle impacts did not appear to affect the wood and Lexan surfaces.

Wood surfaces.- The wood surface tested on wedge configuration W-0 is shown in the photographs presented as figure 17. The panel was made of three boards, as indicated in figure 17(b). The deepest recession of the first board (oak) occurred within areas believed to be turbulence wedges which developed downstream from nicks in the apex of the leading edge. Recession depth within these wedges was as much as 3.2 mm. Diamond-shaped groove patterns were etched within the turbulence wedges but not within the adjacent regions where laminar flow apparently existed. The groove patterns in the oak surface extended onto the front edge of the maple board. Most of the maple surface, however, was charred without groove patterns. Since the average recession of the maple board was 1.6 mm as compared with a recession depth of 3.2 mm in the oak board, the

front edge of the maple board formed a forward-facing ramp. A reasonably uniform recession of 6.4 mm occurred over the last board (pine) which resulted in a substantial rearward-facing step at the downstream edge of the second (maple) board. A prominent diamond-shaped groove pattern was produced over the entire surface of the pine board. The angle between the groove and the stream direction was approximately $28^{\circ}$ on the oak board as compared with a value of approximately $34^{\circ}$ on the pine board.

Lexan surfaces. Lexan was tested on wedges W-1 and W-4, and photographs of the panels after testing are presented as figure 18. The windward side of W-1, which was inclined $34^{\circ}$ to the tunnel flow, is shown in figure 18(a). The uneven, lightly colored area is melted ablative material which flowed along the surface because of the shear forces. Downstream of this area, faint traces of a groove pattern can be seen. Groove patterns were not detected on the leeward side of wedge W-1 which was inclined $26^{\circ}$ to the tunnel flow.

A photograph of zone II of wedge W-4 is shown in figure 18(b). This panel was tested behind a distributed-roughness boundary-layer trip on the leading-edge surface. The groove patterns of figure 18(b) extended over the entire panel and were much deeper than the grooves of figure 18(a). Computed values of the roughness Reynolds number at the top of the trip, based on a method for evaluating roughness effectiveness on planar surfaces reported in reference 13, indicated that the end of boundary-layer transition should have occurred at the location of the trip. Hence, the entire panel of wedge W-4 and other panels placed behind a distributed-roughness trip should have been subjected to turbulent flow.

Teflon surfaces.- The groove pattern in teflon is difficult to discern from photographs because the ablated surface is pure white. Photographs can reveal the patterns distinctly only when a single light source is used which provides shadows that can define the grooves as shown, for example, in the photographs of wedge W-2 in figure 19. A more satisfactory method for showing the groove pattern was to cover the tested teflon surfaces with a thin sheet of white paper and to rub the paper with a graphite block to produce a tracing. This technique produced a good representation of the groove pattern that was amenable to analysis as shown by the tracings of wedges W-2, W-3, and W-4 in figure 20.

These results show that individual groove patterns appear V-shaped and collectively generate an overall diamond pattern, the forward extent of which is affected by the various boundary-layer trips. For example, in zone IV of wedge W-2 shown in figure 20(a), the panel was located behind a metal leading edge with a double grooved strip machined in its surface. The surface pattern of this zone resembled that of the oak board behind the smooth leading edge of wedge W-0, in that, regions defined as turbulence wedges developed downstream of nicks in the leading edge. The onset of V-shaped grooving occurred

inside these regions but not within adjacent regions. Thus, the double grooved strip apparently did not trip the boundary layer over this region. However, the distributed-roughness trip ahead of zones I and II and the double raised strip ahead of zone III produced V-shaped grooving which was more uniformly distributed across the width of these zones and was located farther upstream than in zone IV. (See figs. 19 and 20(a).) Computation of the roughness Reynolds number for the raised strip according to the two-dimensional criteria of reference 13 indicated that, like the distributed roughness elements, the trip height should have subjected the panel in zone III to turbulent flow.

The panel of zones III and IV of wedge W-3 was recessed behind the leading-edge surface to a depth of 0.32 cm, but the results that were obtained were inconclusive. The results obtained from the panels with prefabricated flow disturbances in wedges W-3 and W-4 are discussed subsequently.

The groove patterns obtained on the teflon cones are shown in the developed surface tracings presented as figure 21. The patterns were characterized by longitudinal grooves followed by V-shaped grooves as shown, for example, by the tracing of cone C-1 in figure 21(a). Some of the individual V-shaped patterns also show a longitudinal trailing groove. For cone C-1, the nose tip was smooth, and the longitudinal grooves extended over half the cone length before the onset of the V-shaped grooves. The average location of the onset of the V-shaped grooving corresponded to the location of greatest recession depth which occurred at a distance $l = 43$ cm from the tip as determined from recession data of the present tests reported in reference 7. This location is considered to be the end of transition since the maximum recession depth is indicative of maximum heating. The onset of the V-shaped grooves for the other cone models of figure 21 was located much farther forward than that for cone C-1. For these models, boundary-layer trips were fabricated on the nose tips. According to the method of reference 13 for evaluating roughness effectiveness on axisymmetric surfaces, these trips should have been adequate to insure transition at the trip. Thus, the upstream movement of the onset of V-shaped grooving is associated with the upstream movement of the location of boundary-layer transition. Consequently, this result supports the belief that a turbulent boundary layer is required for the existence of a V-shaped groove pattern. The most extensive grooving was obtained on cones C-4 and C-7 as shown in figures 21(d), 21(g), and 22. Because cone C-4 was tested at an angle of attack of $4^{\circ}$ and cone C-7 was actually an extended test of cone C-2, considerable surface recession, which resulted in the formation of a rearward-facing step, occurred on these models downstream of the nose tip. This step may have increased the vorticity of the flow, and consequently, may have contributed to the downstream development of the more extensive groove pattern. The other cone models also showed a rearward-facing step behind the nose tip but not as deep as those on cones C-4 and C-7.

Measurements of the groove angle taken from the wedge and cone tracings of figures 20 and 21 are presented as a function of local free-stream Mach number in figure 23. The present results for the cones and the wedges at $\alpha = 0$ and the windward and leeward sides of cone C-4 indicate a data scatter of $5^{\circ}$ above and below the Mach angle curve. These results substantiate the Mach number correlation with groove angle suggested by a number of investigators. (See refs. 3 to 6.)

## Effects of Different Flow Disturbances

The grooving patterns that formed behind the prefabricated flow disturbances in teflon cones C-5 and C-6 and teflon wedge configurations W-3 and W-4 are presented as figures 24 and 25. A photograph of the disturbance location and the corresponding tracing is presented for each disturbance. A local surface ablation pattern was produced by each of the disturbances. In most instances, the pins used for the disturbances were blown out during testing (disturbances 4, 5, 6, 7, and 9 of C-5; disturbances 4 and 12 of C-6; and disturbance 4 of W-4). Therefore, the grooving pattern from such disturbances was not definitely established. The 1.6-mm-diameter hole (disturbance 1 of C-5, fig. 24(a)) produced a simple double-V-shaped groove pattern. The larger hole sizes (for example, disturbances 2, 3, and 8 of C-5, figs. 24(a) and 24(c)) produced V-shaped patterns with longitudinal grooves which apparently resulted from trailing vortices. The patterns produced by the slots of various lengths (disturbances 5, 6, 7, 8, and 9 of C-6, fig. 24(f)) were also characterized by pronounced longitudinal trailing grooves which increased in depth with slot length.

Various arrangements of disturbance holes were tested including lateral spacing (disturbances 10, 11, and 12 of C-5, fig. 24(d), and disturbances 1, 2, 3, and 5 of W-4, fig. 25(b)), longitudinal spacing (disturbances 1, 2, and 3 of C-6, fig. 24(e)), and area spacing (disturbances 1, 2, 3, and 4 of W-3, fig. 25(a)). In each comparison, one of the arrays of holes was spaced to produce the characteristic spacing of the aerodynamic grooving of the respective surfaces without prefabricated disturbances (disturbance 10 of C-5, fig. 24(d); disturbance 1 of C-6, fig. 24(e); disturbance 3 of W-3, fig. 25(a); and disturbance 1 of W-4, fig. 25(b)). Each of the other arrays of holes was either double or half this characteristic spacing except disturbance 4 of W-3 (fig. 25(a)) and disturbance 5 of W-4 (fig. 25(b)), which had random and varied spacing, respectively. Although a wide variety of disturbance spacing was tested, the predominant groove pattern produced was always the same. Another important observation is that groove patterns did not propagate laterally from the disturbance. For example, see the longitudinally spaced disturbance holes in figure 24(e).

## CONCLUDING REMARKS

An investigation was made in the Langley 8-foot high-temperature structures tunnel to study the formation of ablation patterns on teflon surfaces of large cone and wedge models and on wood and Lexan surfaces of wedge models immersed in a high-enthalpy hypersonic stream. The tests were conducted at a Mach number of 7.4, at total temperatures between 1810 K and 1970 K, at stream enthalpies between 2.34 and 2.55 MJ/kg, and at unit Reynolds numbers between $0.35 \times 10^6$ and $0.55 \times 10^6$ per meter. Also, nonablative calibration results were obtained on a similar cone and on wedge insert plates to indicate the heating and pressure levels on the cones and the heating on the wedges. It was concluded that diamond-shaped groove patterns developed only in the presence of turbulent flow, that rearward-facing steps appeared to cause more extensive grooving patterns, and that the angle between the grooves and the local flow direction was approximately equal to the local Mach angle with a scatter of $\pm 5^{\circ}$. The following conclusions were reached after studying the effects of prefabricated flow disturbances on groove patterns: (1) Small surface holes produced localized groove patterns; whereas, larger holes produced strong trailing vortices which grooved the surface in the stream direction. (2) The patterns from disturbances had a characteristic groove spacing which was independent of disturbance spacing. (3) The patterns from disturbances did not propagate laterally.

Langley Research Center,
National Aeronautics and Space Administration,
Hampton, Va., April 13, 1970.

## REFERENCES


1. Canning, Thomas N.; Wilkins, Max E.; and Tauber, Michael E.: Boundary-Layer Phenomena Observed on the Ablative Surfaces of Cones Recovered After Flights at Speeds up to 7 km/sec. Fluid Physics of Hypersonic Wakes, Vol. 2, AGARD CP No. 19, May 1967.

2. Canning, Thomas N.; Wilkins, Max E.; and Tauber, Michael E.: Ablation Patterns on Cones Having Laminar and Turbulent Flows. AIAA J., vol. 6, no. 1, Jan. 1968, pp. 174-175.

3. Larson, H. K.; and Mateer, G. G.: Cross-Hatching – A Coupling of Gas Dynamics With the Ablation Process. AIAA Pap. No. 68-670, June 1968.

4. Canning, Thomas N.; Tauber, Michael E.; Wilkins, Max E.; and Chapman, Gary T.: Orderly Three-Dimensional Processes in Turbulent Boundary Layers on Ablating Bodies. Hypersonic Boundary Layers and Flow Fields, AGARD CP No. 30, May 1968, pp. 6-1 – 6-14.

5. Williams, E. P.: Experimental Studies of Ablation Surface Patterns and Resulting Roll Torques. AIAA Pap. No. 69-180, Jan. 1969.

6. Laganelli, A. L.; and Nestler, D. E.: Surface Ablation Patterns: A Phenomenology Study. AIAA Pap. No. 68-671, June 1968.

7. Anon.: RVTO Roll Phenomenology. Vol. 2. Doc. No. 68SD809 (Contract AF 04(694)-914), Re-Entry Syst. Dep., Gen. Elec. Co., July 23, 1968.

8. Comm. on Metric Pract.: ASTM Metric Practice Guide. NBS Handbook 102, U.S. Dep. Com., Mar. 10, 1967.

9. Eckert, Ernst R. G.: Survey on Heat Transfer at High Speeds. ARL 189 (Contract AF 33(616)-2214), U.S. Air Force, Dec. 1961.

10. Laganelli, A. L.; and Weisz, S.: Ablation Surface Pattern Study – Conducted in Langley 8 Foot High Temperature Structures Tunnel. No. 67SD7327, Missile Space Div., Gen. Elec. Co., Dec. 13, 1967.

11. Leyhe, E. W.; and Howell, R. R.: Calculation Procedure for Thermodynamic, Transport, and Flow Properties of the Combustion Products of a Hydrocarbon Fuel Mixture Burned in Air With Results for Ethylene-Air and Methane-Air Mixtures. NASA TN D-914, 1962.

12. Kays, W. M.: Convective Heat and Mass Transfer. McGraw-Hill Book Co., Inc., c.1966.

13. Potter, J. Leith; and Whitfield, Jack D.: Boundary-Layer Transition Under Hypersonic Conditions. Recent Developments in Boundary Layer Research, Pt. III, AGARDograph 97, May 1965, pp. 1-62.

TABLE I.- LOCATION OF INSTRUMENTATION ON CALIBRATION CONE

(a) Slug calorimeters and pressure orifices

| $l$, cm | $\phi$, deg |
|---|---|
| Slug calorimeters | |
| 10.4 | 0 |
| 14.0 | 0 |
| 17.8 | 0 |
| 21.6 | 0 |
| 25.4 | 0 |
| 29.2 | 0 |
| 33.0 | 0 |
| 36.8 | 0 |
| 40.6 | 0 |
| 44.5 | 0 |
| 48.3 | 0 |
| 52.1 | 0 |
| 55.9 | 0 |
| 10.4 | 180 |
| 14.0 | 180 |
| 21.6 | 180 |
| 25.4 | 180 |
| 29.2 | 180 |
| 33.0 | 180 |
| 36.8 | 180 |
| 40.6 | 180 |
| 44.5 | 180 |
| 48.3 | 180 |
| 55.9 | 180 |
| Pressure orifices | |
| 17.8 | 90 |
| 17.8 | 180 |
| 17.8 | 270 |
| 52.1 | 45 |
| 52.1 | 90 |
| 52.1 | 135 |
| 52.1 | 180 |
| 52.1 | 225 |
| 52.1 | 220 |
| 52.1 | 315 |

(b) Boundary-layer-rake pitot probes

| $\phi$, deg | y, mm |
|---|---|
| 126.00 | 7.62 |
| 127.12 | 6.35 |
| 128.25 | 5.85 |
| 129.38 | 5.08 |
| 130.50 | 4.70 |
| 131.62 | 4.45 |
| 132.75 | 3.56 |
| 133.88 | 3.30 |
| 135.00 | 2.92 |
| 145.00 | 4.70 |
| 146.12 | 4.70 |
| 147.25 | 4.83 |
| 148.38 | 4.83 |
| 149.50 | 4.70 |
| 150.62 | 4.70 |
| 151.75 | 4.70 |
| 152.88 | 4.70 |
| 154.00 | 4.70 |
| 306.00 | 9.91 |
| 307.12 | 8.77 |
| 308.25 | 7.62 |
| 309.38 | 6.61 |
| 310.50 | 6.10 |
| 311.62 | 5.08 |
| 312.75 | 4.70 |
| 313.88 | 4.58 |
| 315.00 | 4.32 |
| 325.00 | 6.10 |
| 326.12 | 6.10 |
| 327.25 | 6.10 |
| 328.38 | 6.10 |
| 329.50 | 6.10 |
| 330.62 | 5.97 |
| 331.75 | 6.10 |
| 332.88 | 6.10 |
| 334.00 | 6.10 |

TABLE II.- POSITION OF THERMOCOUPLES ON STEEL INSERT PLATES ON ABLATIVE WEDGES

| $l$, cm | w, cm |
|---|---|
| Model W-2 (zones I and II) | |
| 30.5 | 26.0 |
| 32.3 | 18.6 |
| 34.2 | 11.2 |
| 35.9 | 3.7 |
| 37.8 | -3.7 |
| 39.6 | -11.2 |
| 41.3 | -18.6 |
| 43.2 | -26.0 |
| 43.2 | -17.3 |
| 43.2 | -8.7 |
| 43.2 | 0 |
| 43.2 | 8.7 |
| 43.2 | 17.3 |
| 43.2 | 26.0 |
| Model W-4 (zones I and II) | |
| 45.7 | -2.5 |
| 45.7 | 0 |
| 45.7 | 2.5 |
| 48.3 | 1.7 |
| 50.8 | .8 |
| 53.4 | 0 |
| 55.9 | -.8 |
| 58.5 | -1.7 |
| 61.0 | -2.5 |
| 61.0 | 0 |
| 61.0 | 2.5 |

TABLE III.- DESCRIPTION OF FLOW DISTURBANCES

(a) Ablative wedge models

| Disturbance | Description |
|---|---|
| | Model W-3 |
| 1 | 28 holes, 1.6 mm diam, 1.6 mm deep, w' = 2.04 cm, $l'$ = 2.16 cm |
| 2 | 233 holes, 1.6 mm diam, 1.6 mm deep, w' = 5.1 mm, $l'$ = 5.4 mm |
| 3 | 105 holes, 1.6 mm diam, 1.6 mm deep, w' = 1.02 cm, $l'$ = 1.08 mm |
| 4 | 100 holes, 1.6 mm diam, 1.6 mm deep, random spacing |
| | Model W-4 |
| 1 | 6 holes, 1.6 mm diam, 1.6 mm deep, spaced 9.5 mm, perpendicular to flow |
| 2 | 6 holes, 1.6 mm diam, 1.6 mm deep, spaced 4.8 mm, perpendicular to flow |
| 3 | 6 holes, 1.6 mm diam, 1.6 mm deep, spaced 1.91 cm, perpendicular to flow |
| 4 | 6 pins, 1.6 mm diam, 1.6 mm high, spaced 9.5 mm, perpendicular to flow |
| 5 | 19 holes, 1.6 mm diam, 1.6 mm deep, spaced exponentially, perpendicular to flow |
| 6 | 3 holes, 3.2 mm diam, 3.2 mm deep, spaced 9.5 mm, perpendicular to flow |
| 7 | 3 holes, 3.2 mm diam, 3.2 mm deep, spaced 1.43 cm, perpendicular to flow |
| 8 | 3 holes, 3.2 mm diam, 3.2 mm deep, spaced 9.5 mm, perpendicular to flow |
| 9 | 3 holes, 3.2 mm diam, 3.2 mm deep, spaced 1.43 cm, perpendicular to flow |

(b) Ablative cone models

| Disturbance | Description |
|---|---|
| | Model C-5 |
| 1 | 1 hole, 1.6 mm diam, 1.6 mm deep |
| 2 | 1 hole, 3.2 mm diam, 3.2 mm deep |
| 3 | 1 hole, 1.03 cm diam, 6.4 mm deep |
| 4 | 1 pin, 3.2 mm diam, flush with surface |
| 5 | 1 pin, 3.2 mm diam, 0.38 mm high |
| 6 | 1 pin, 3.2 mm diam, 1.6 mm high |
| 7 | 1 pin, 3.2 mm diam, 3.2 mm high |
| 8 | Slot, round leading edge, 1.11 cm wide, 1.83 cm long, 3.2 mm deep, $45^{\circ}$ swept rear wall |
| 9 | 1 pin, 3.2 mm diam, 3.2 mm high, swept $45^{\circ}$ |
| 10 | 3 holes, 3.2 mm diam, 3.2 mm deep, spaced 9.5 mm, perpendicular to flow |
| 11 | 3 holes, 3.2 mm diam, 3.2 mm deep, spaced 4.8 mm, perpendicular to flow |
| 12 | 3 holes, 3.2 mm diam, 3.2 mm deep, spaced 1.91 cm, perpendicular to flow |
| | Model C-6 |
| 1 | 6 holes, 1.6 mm diam, 1.6 mm deep, spaced 1.91 cm, parallel to flow |
| 2 | 6 holes, 1.6 mm diam, 1.6 mm deep, spaced 9.5 mm, parallel to flow |
| 3 | 6 holes, 1.6 mm diam, 1.6 mm deep, spaced 3.81 cm, parallel to flow |
| 4 | 6 pins, 1.6 mm diam, 1.6 mm high, spaced 1.91 cm, parallel to flow |
| 5 | Hemispherical hole, 9.5 mm diam |
| 6 | Semicircular slot, 9.5 mm diam, 1.27 cm long, parallel to flow |
| 7 | Semicircular slot, 9.5 mm diam, 1.59 cm long, parallel to flow |
| 8 | Semicircular slot, 9.5 mm diam, 1.91 cm long, parallel to flow |
| 9 | Semicircular slot, 9.5 mm diam, 2.86 cm long, parallel to flow |
| 10 | 3 adjacent semicircular slots, 9.5 mm diam, 10.16 cm long, parallel to flow |
| 11 | 3 holes, 3.2 mm diam, 3.2 mm deep, spaced $7.5^{\circ}$ offset and 7.62 cm parallel to flow |
| 12 | 3 pins, 3.2 mm diam, flush with surface, spaced $7.5^{\circ}$ offset and 7.62 cm parallel to flow |

TABLE IV.- SUMMARY AND IDENTIFICATION OF TESTS

(a) Cones

| Model | $p_t$, $MN/m^2$ (a) | $T_t$, K | $\alpha$, deg | t, s | Nose tip | Test material | Remarks |
|---|---|---|---|---|---|---|---|
| Calibration | 15.4 | 1910 | 0 | 5.05 | Smooth | | Calibration cone |
| C-1 | 15.2 | 1920 | 0 | 19.99 | Smooth | Teflon | |
| C-2 | 15.4 | 1920 | 0 | 24.55 | Single raised ring | Teflon | |
| C-3 | 18.7 | 1960 | 0 | 24.47 | Double raised ring | Teflon | |
| C-4 | 17.7 | 1970 | 4 | 26.01 | Distributed roughness | Teflon | |
| C-5 | 17.9 | 1810 | 0 | 22.70 | Double raised ring | Teflon | With flow disturbances |
| C-6 | 18.5 | 1880 | 0 | 27.19 | Double raised ring | Teflon | With flow disturbances |
| C-7 | 18.9 | 1820 | 0 | 28.80 | Double raised ring | Teflon | Extended test of C-2 |

(b) Wedges

| Model | $p_t$, $MN/m^2$ (a) | $T_t$, K | $\alpha$, deg | t, s | Leading edge | | | | Test material | | | | Remarks |
|---|---|---|---|---|---|---|---|---|---|---|---|---|---|
| | | | | | I | II | III | IV | I | II | III | IV | |
| W-0 | 13.9 | 1960 | 0 | 9.80 | Smooth | | | | Wood | | Teflon | | |
| W-1 | 13.5 | 1960 | 4 | 5.10 | Smooth | | | | Lexan | | | | |
| W-1 | 15.1 | 1920 | 4 | 9.00 | Smooth | | | | Lexan | | | | |
| W-2 | 18.1 | 1840 | 0 | 6.45 | Distributed roughness | | Double raised strip | Double groove strip | Teflon | | | | Insert plate zones I and II |
| W-2 | 17.9 | 1920 | 0 | 24.59 | Distributed roughness | | Double raised strip | Double groove strip | Teflon | | | | |
| W-3 | 18.3 | 1840 | 0 | 29.02 | Double raised strip | | Distributed roughness | Smooth | Teflon | | | | Flow disturbances, zones I and II panel recessed, zones III and IV |
| W-4 | 18.2 | 1830 | 0 | 19.27 | Distributed roughness | | Double raised strip | | Teflon | Lexan | Teflon | | Flow disturbances, zones I, III, and IV, insert plate zones I and II |

[a]Conversion: $p_t$ $(MN/m^2) \times 145.2 = p_t$ (psia)

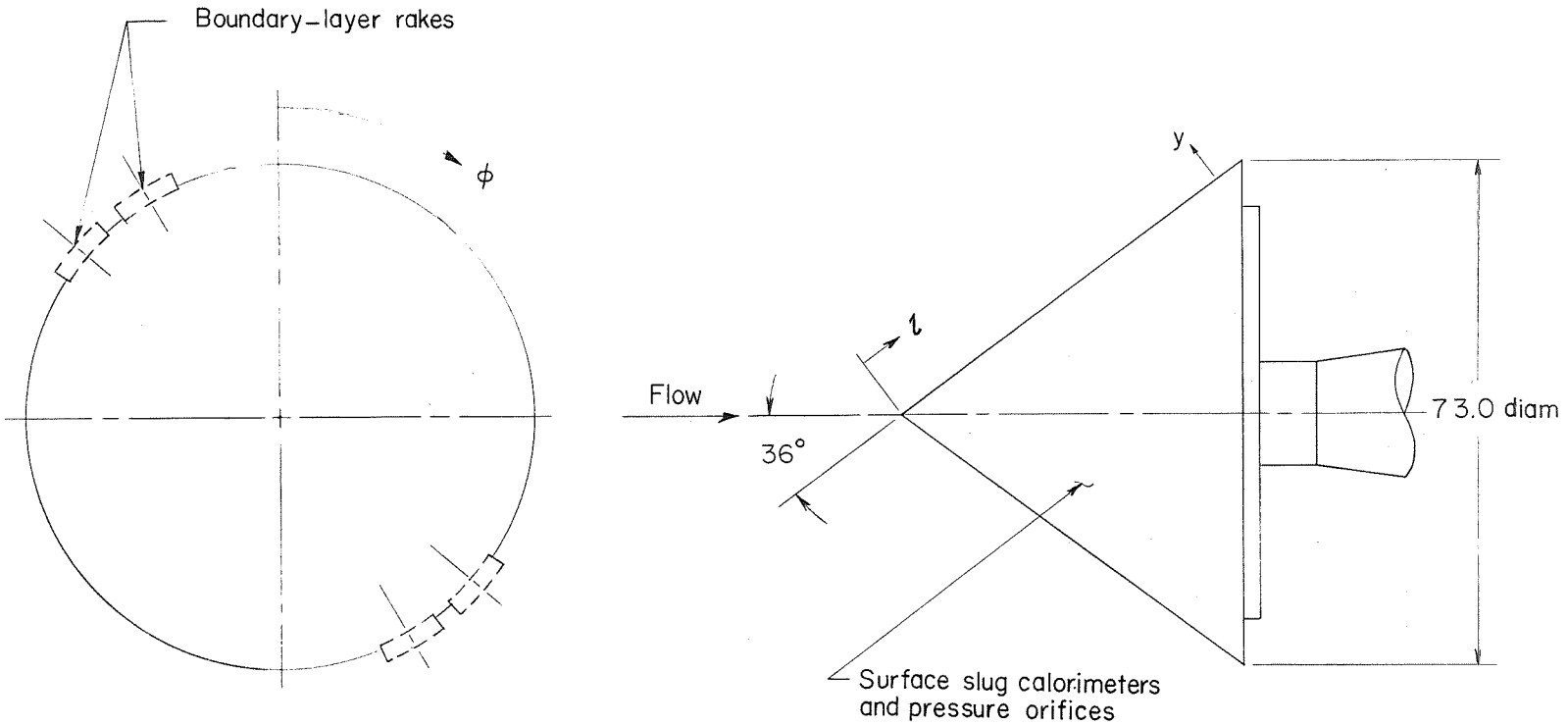


Figure 1.- Calibration cone. All dimensions are in centimeters. Positions of boundary-layer-rake probes, surface-pressure orifices, and slug calorimeters are given in table I.

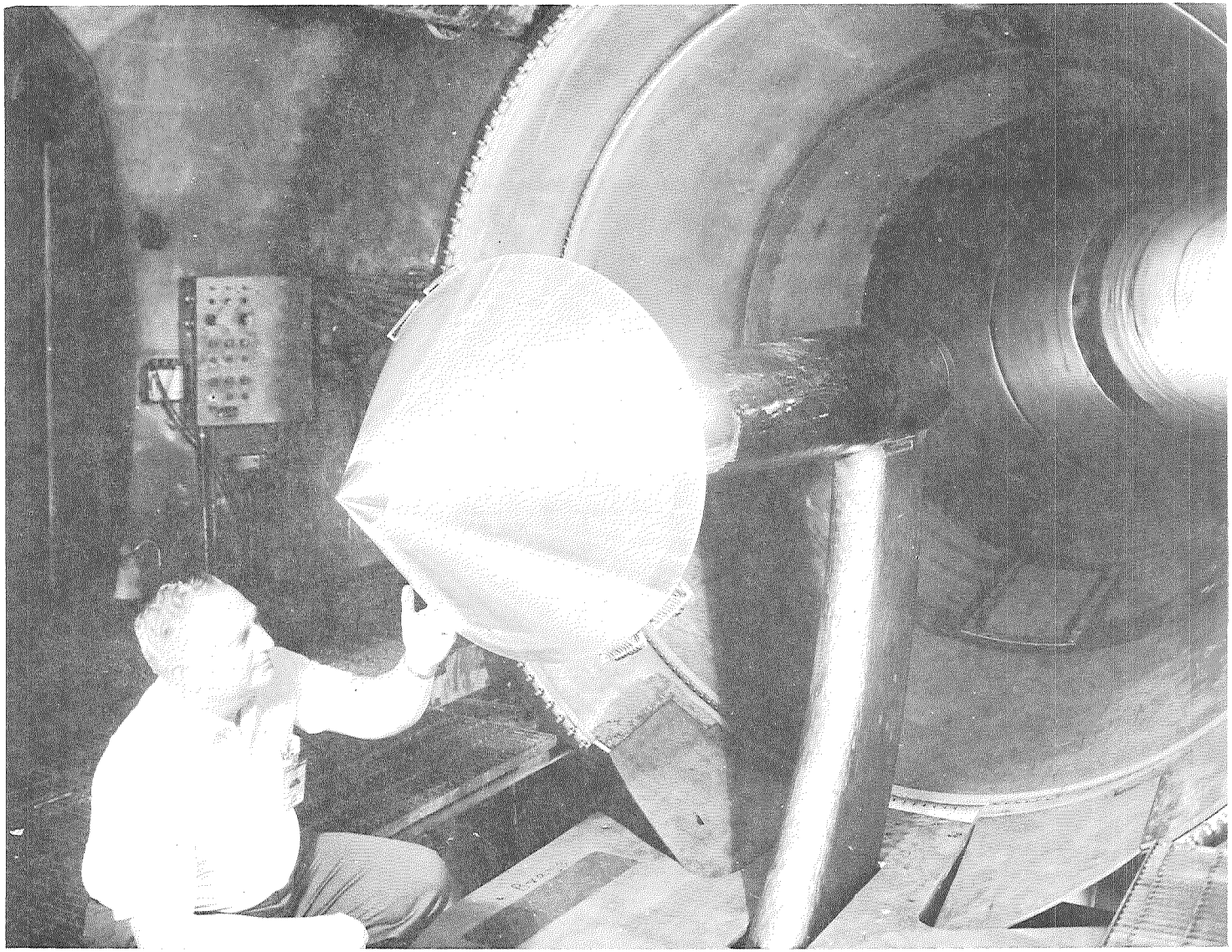

Figure 2.- 36° calibration cone. L-68-2604

Figure 3.- Boundary-layer rakes on $36^0$ calibration cone. L-68-2608

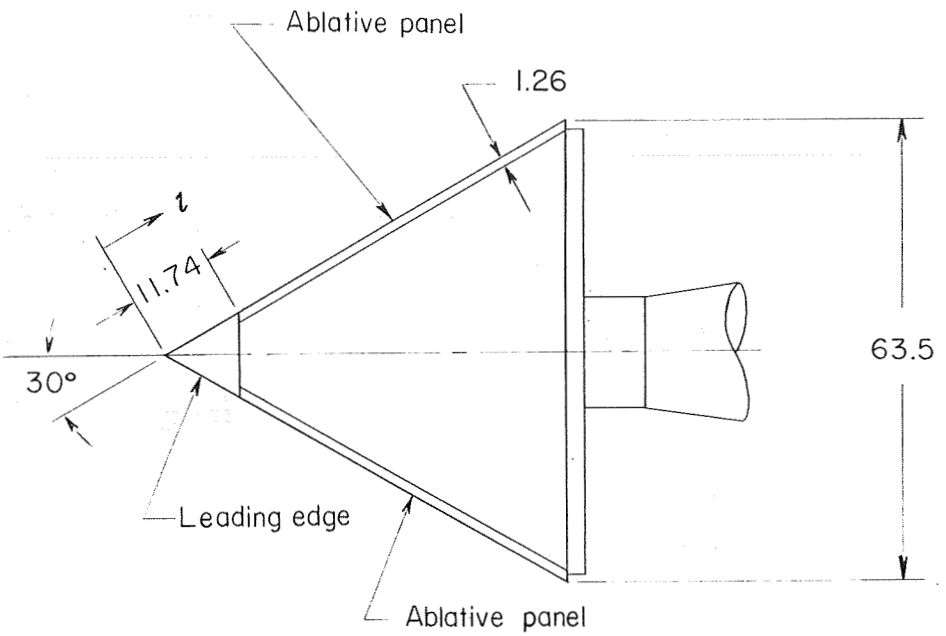


Top view

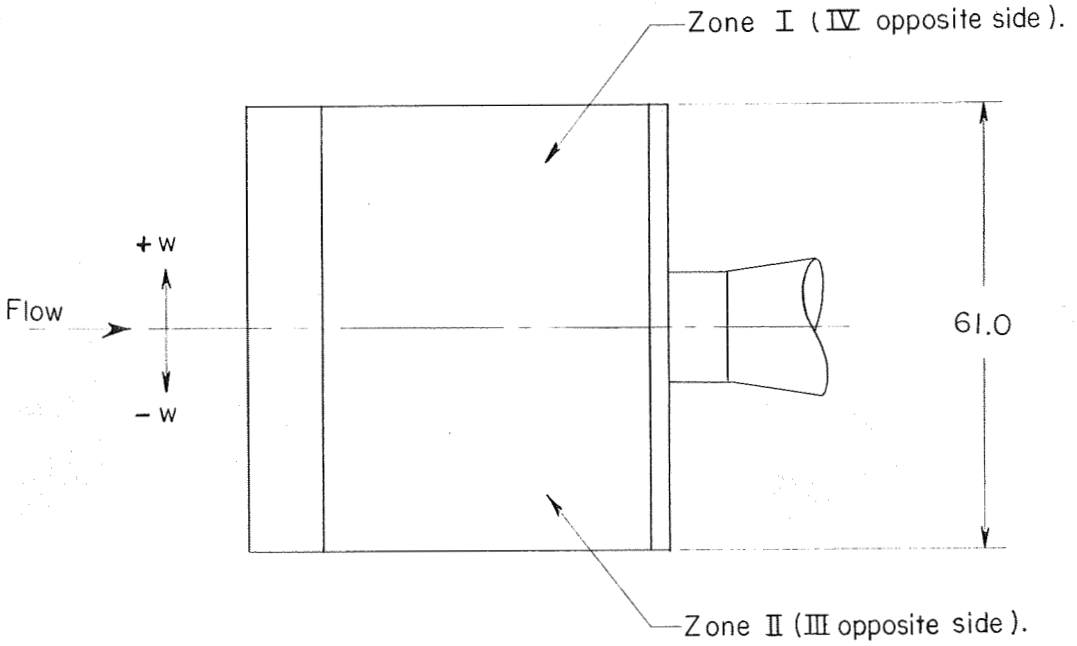


Side view

Figure 4.- Ablative wedge model. All dimensions are in centimeters.

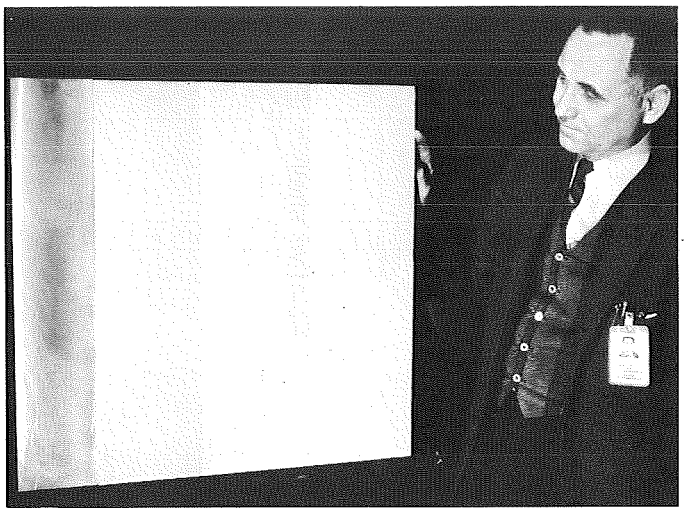

(a) W-0; zones I and II. L-68-1840

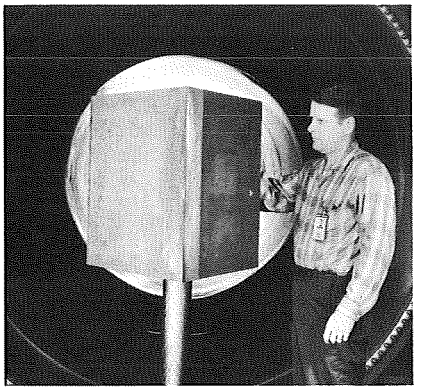

(b) W-1. L-68-1821

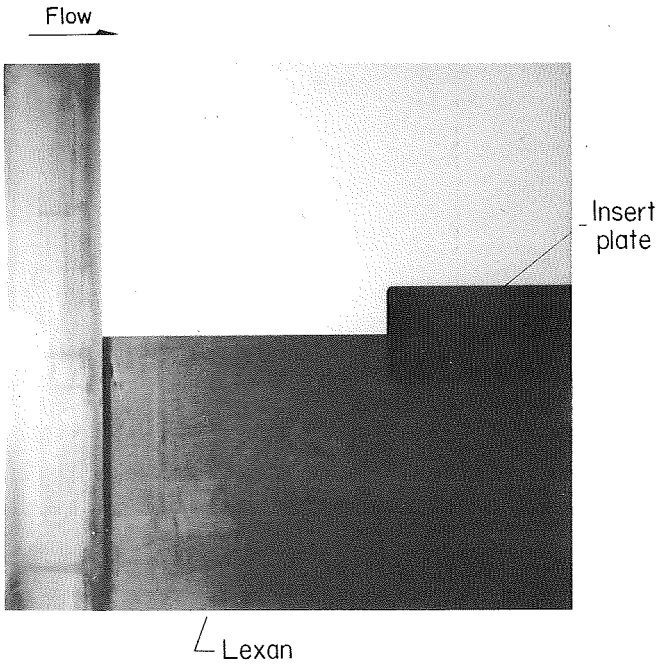


(c) W-4; zones I and II. L-68-4283

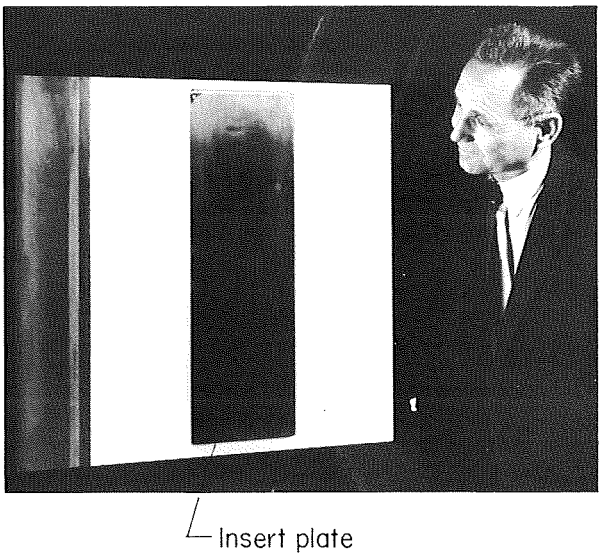


(d) W-2; zones I and II. L-68-3475

Figure 5.- Typical ablation panels on $30^{0}$ wedge.

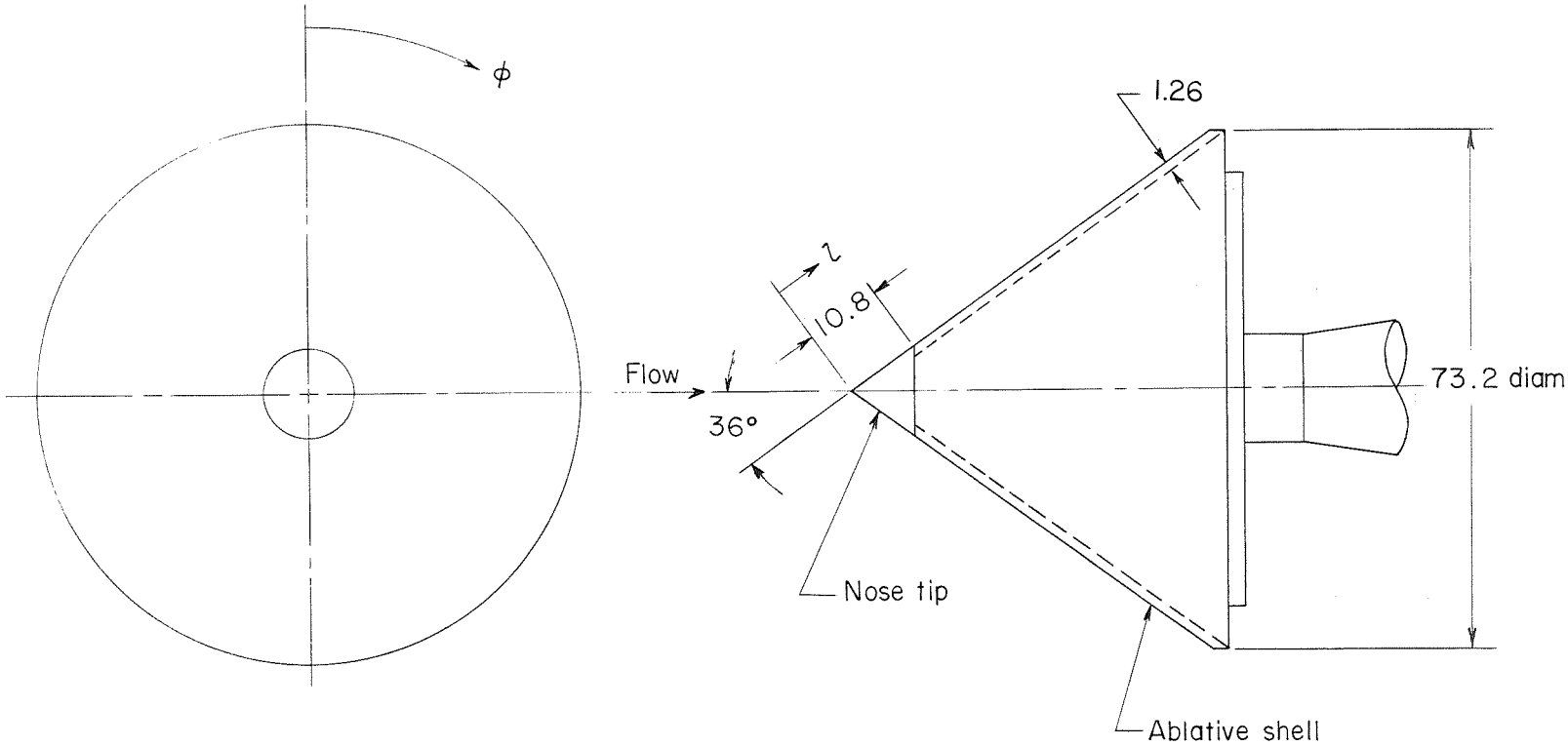


Figure 6.- Ablative cone model. All dimensions are in centimeters.

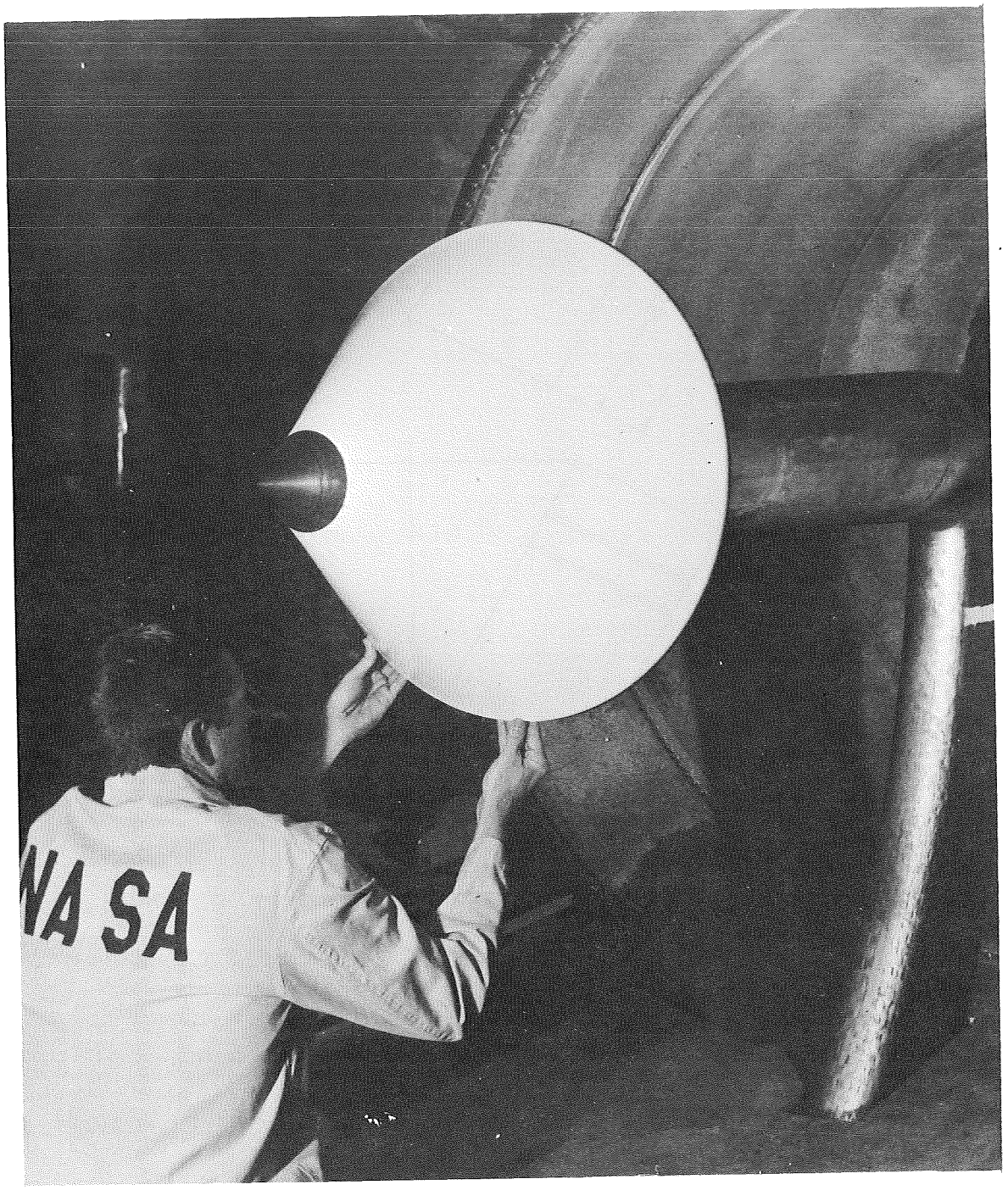


Figure 7.- Typical 36$^0$ teflon cone. L-68-5342

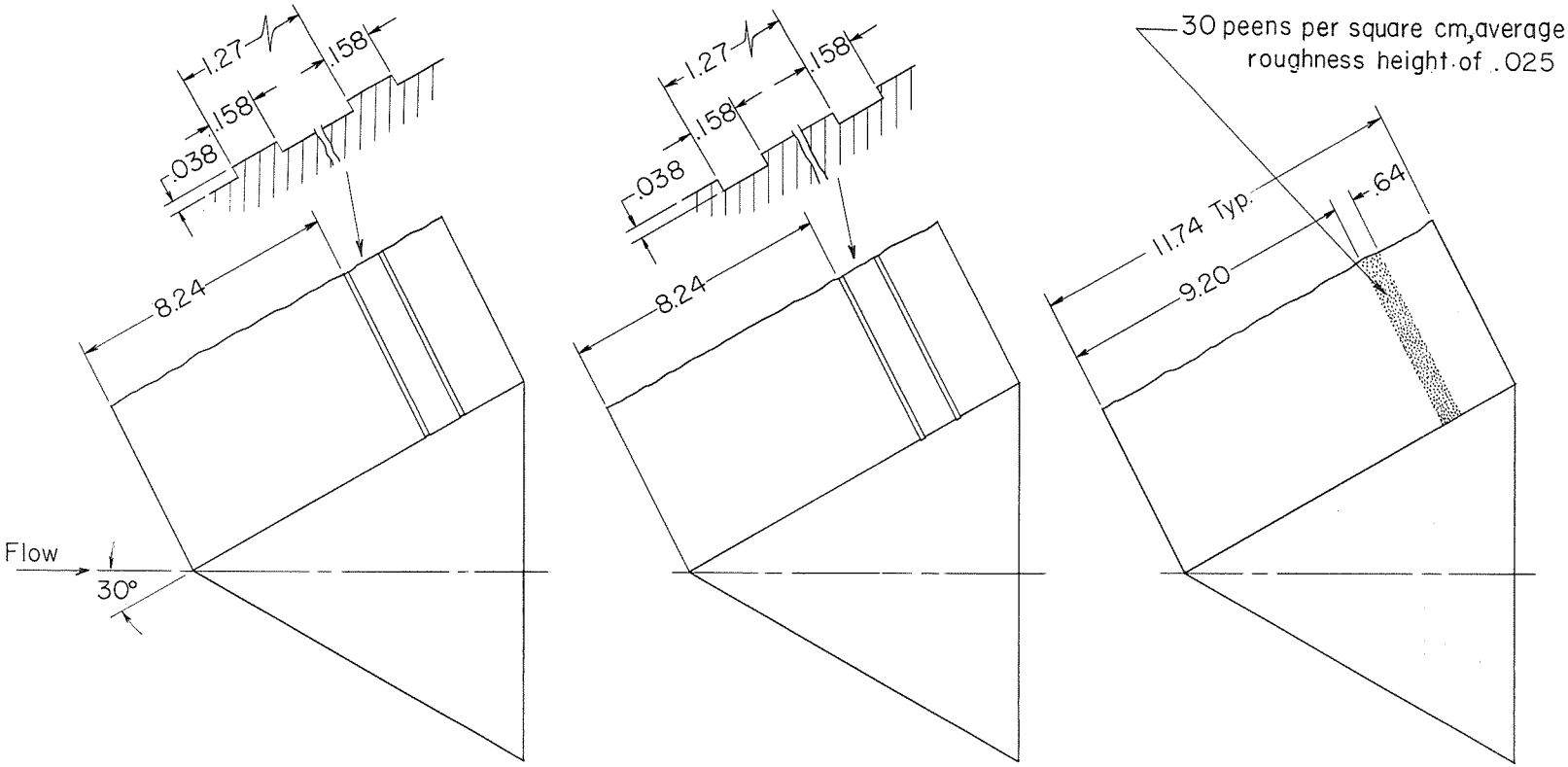


(a) Double raised strip. (b) Double grooved strip. (c) Distributed roughness.

Figure 8.- Various types of boundary-layer trips used on leading edges of ablative wedge models. All dimensions are in centimeters.

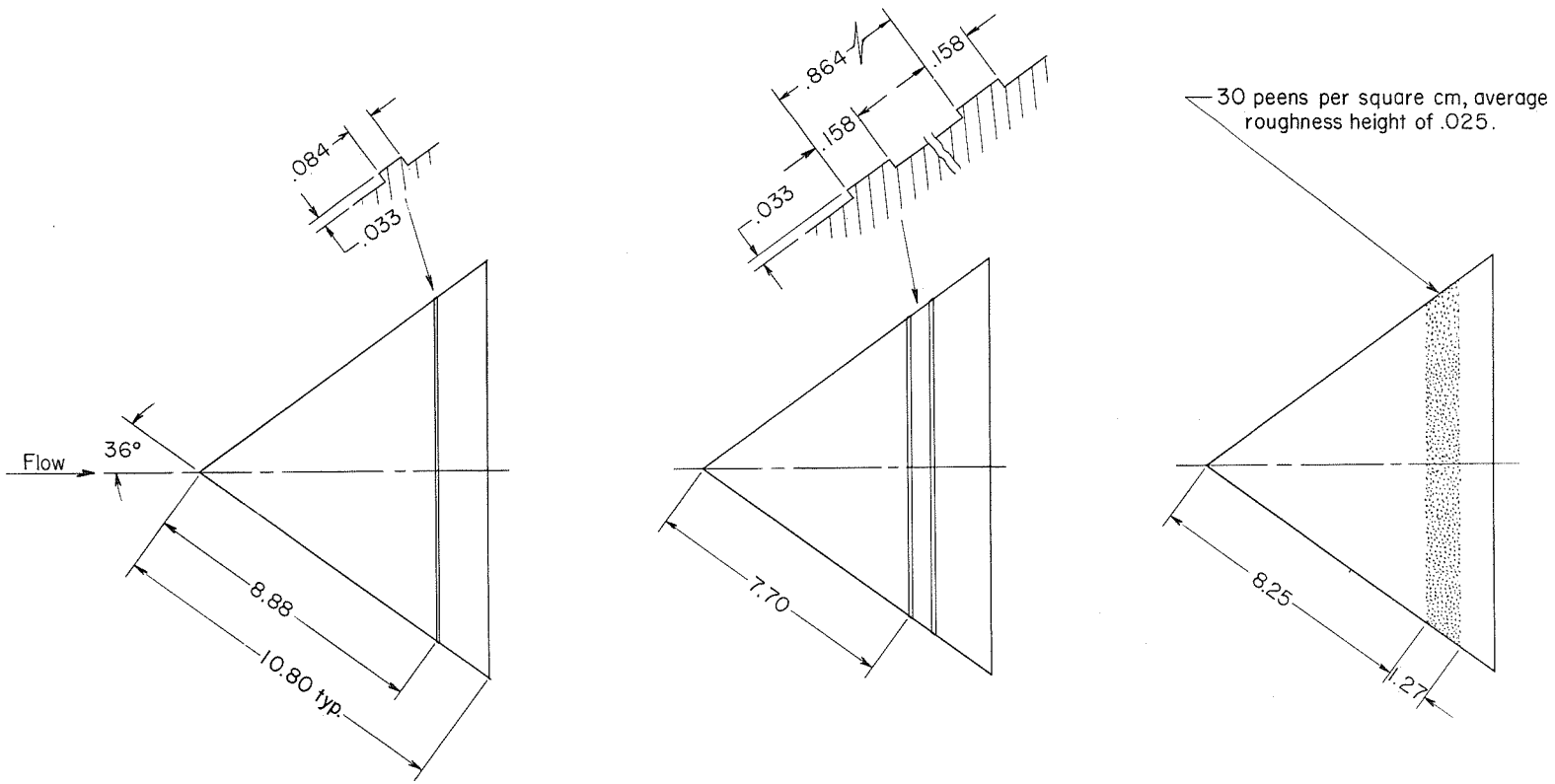


(a) Single raised ring. (b) Double raised ring. (c) Distributed roughness.

Figure 9.- Various types of boundary-layer trips used on nose tips of ablative cone models. All dimensions are in centimeters.


Figure 10.- Two nose tips with boundary-layer trips.

L-68-4834

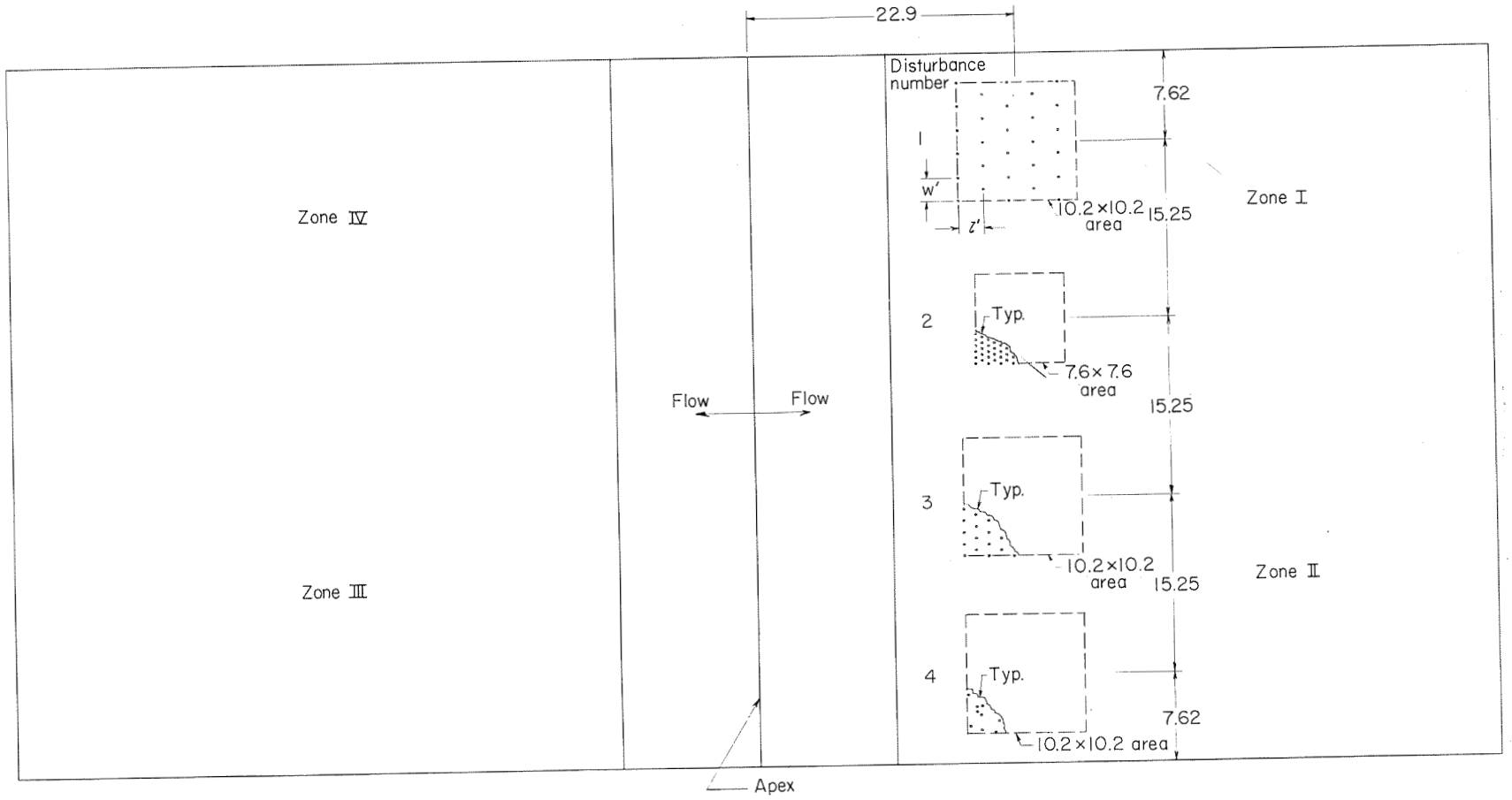


(a) W-3.

Figure 11.- Developed surfaces of the ablative wedge surfaces with prefabricated flow disturbances. All dimensions are in centimeters.

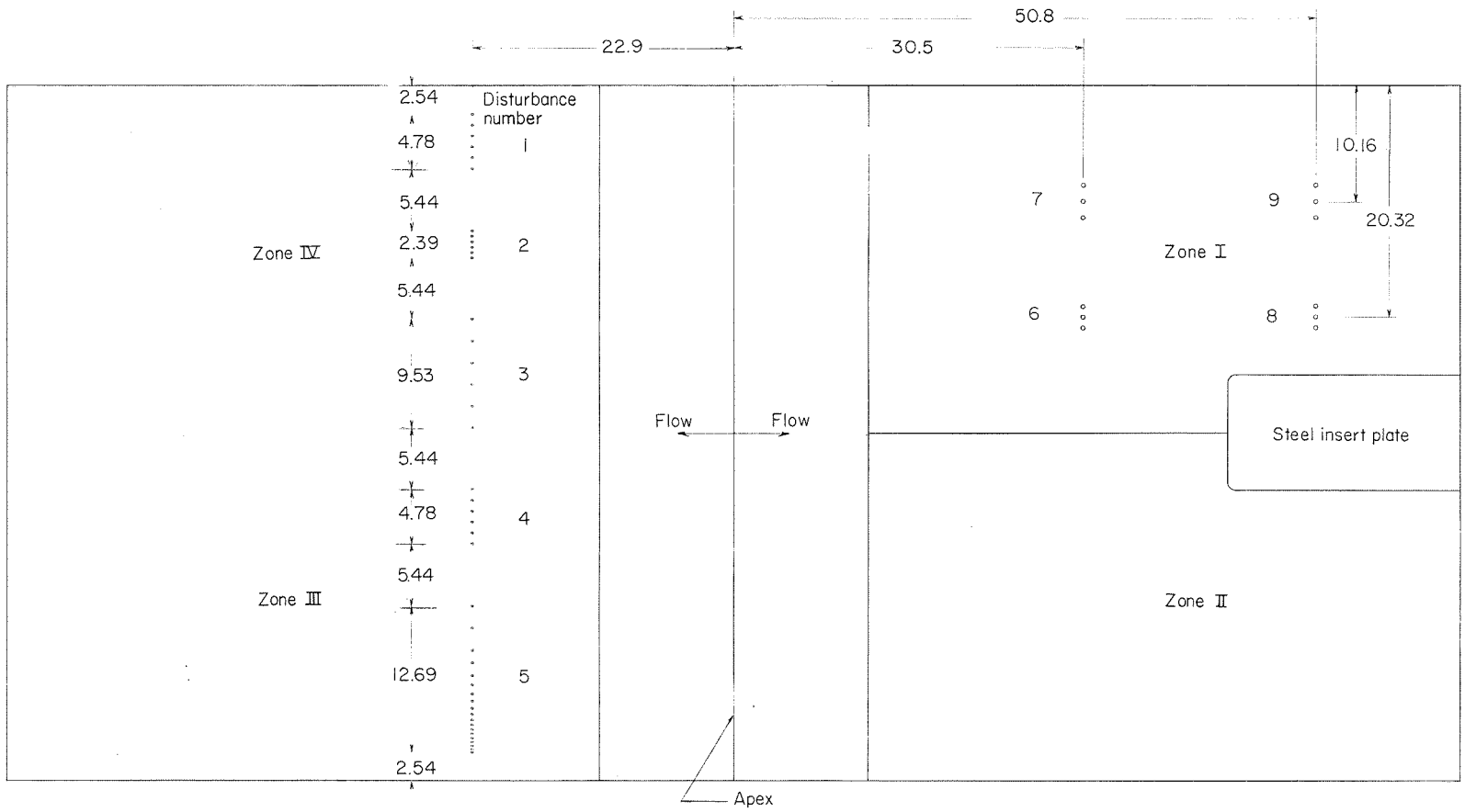


(b) W-4.

Figure 11.- Concluded.

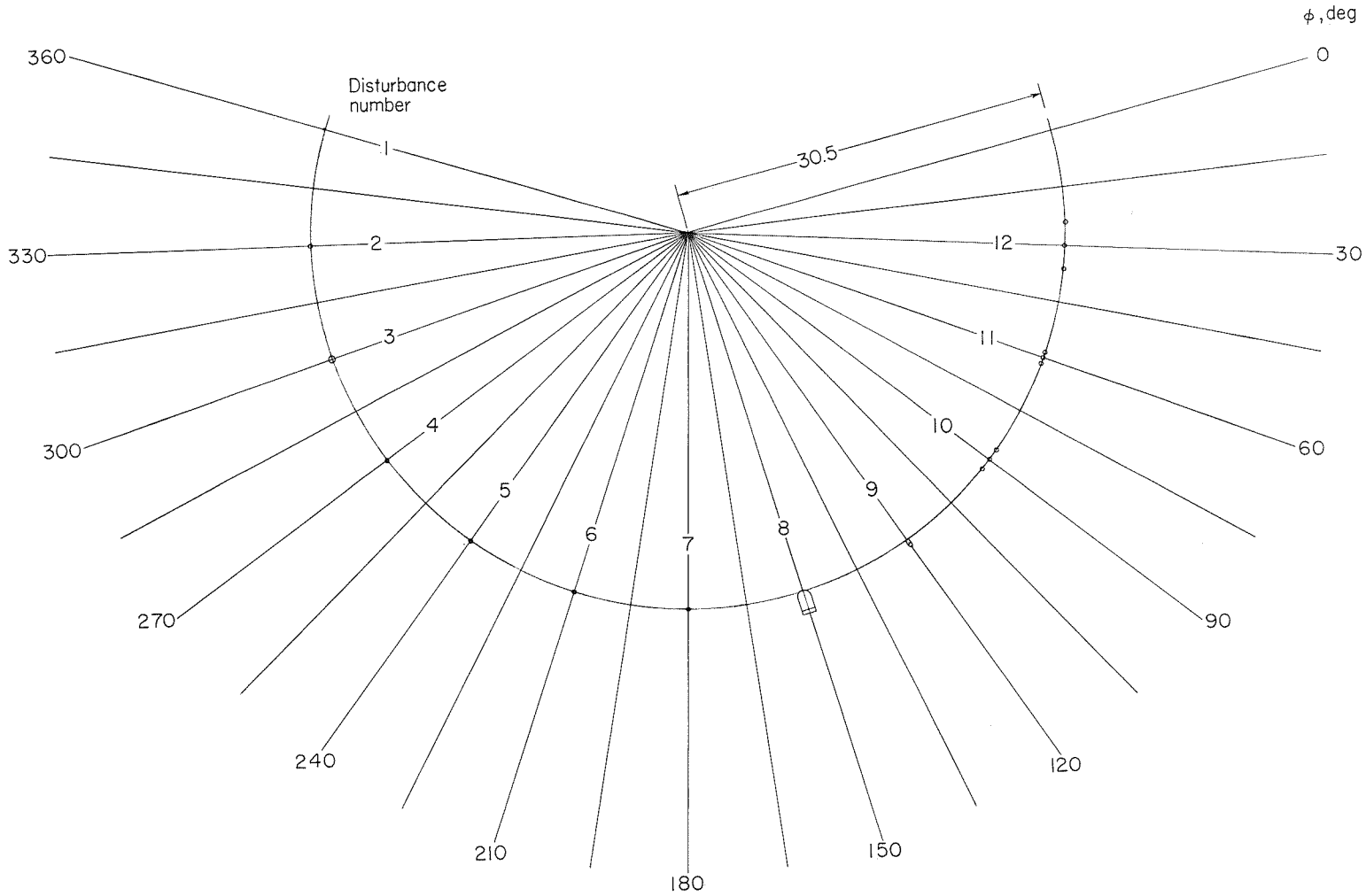


(a) C-5.

Figure 12.- Developed surfaces of ablative cone shells with prefabricated flow disturbances. Flow into paper; all dimensions are in centimeters.

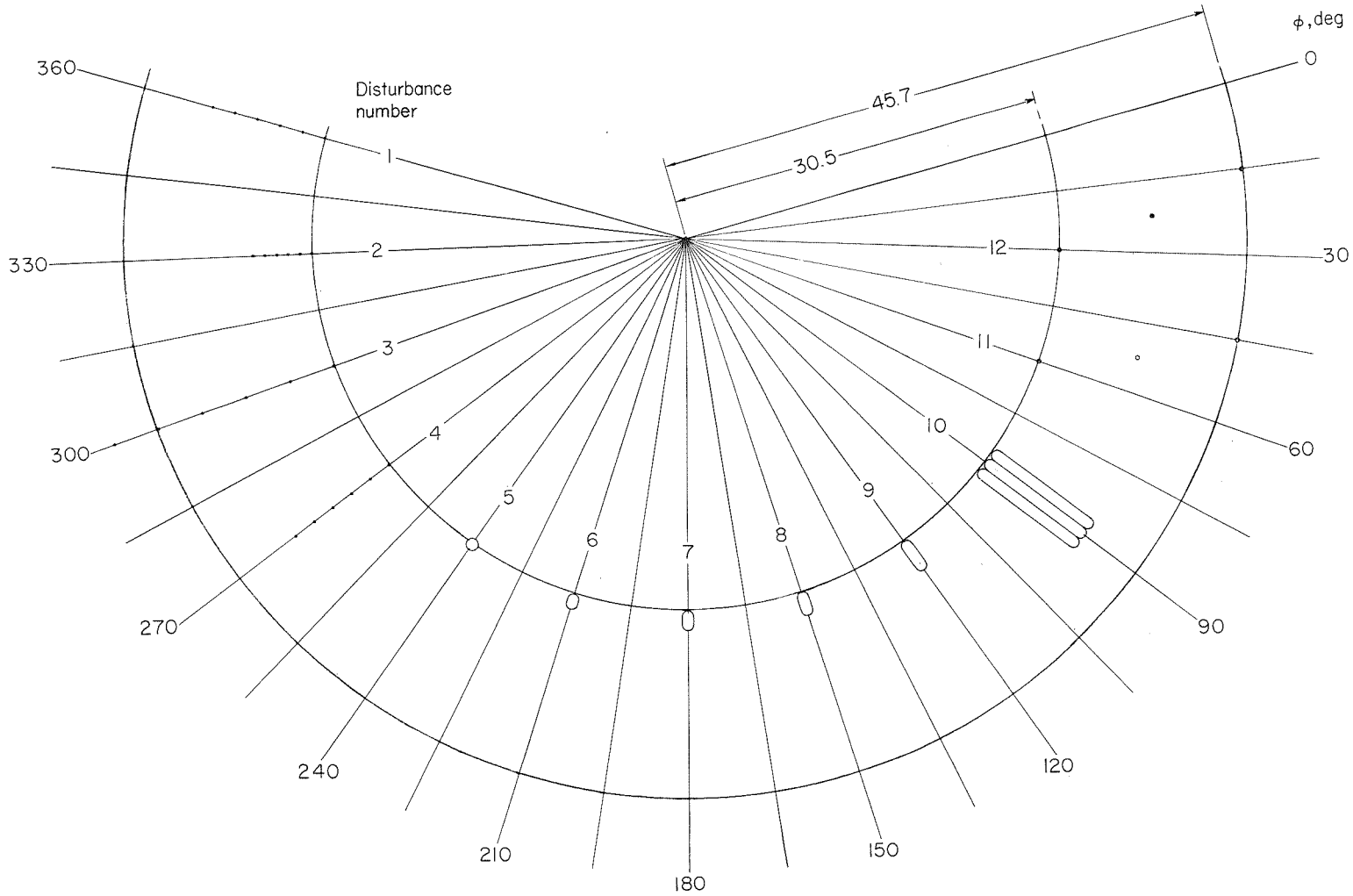


(b) C-6.

Figure 12.- Concluded.

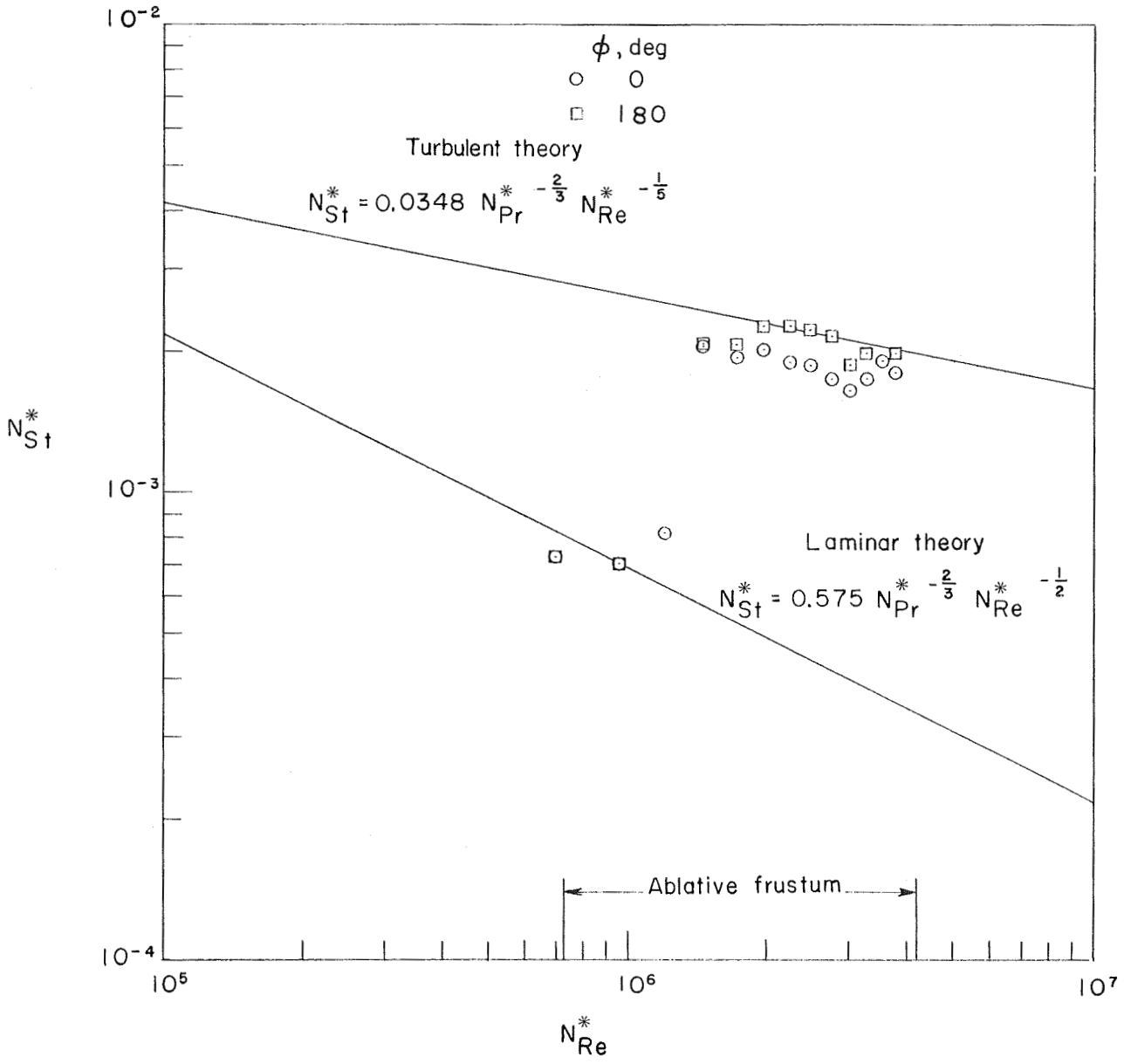


Figure 13.- Aerodynamic heating distribution on $36^0$ calibration cone.

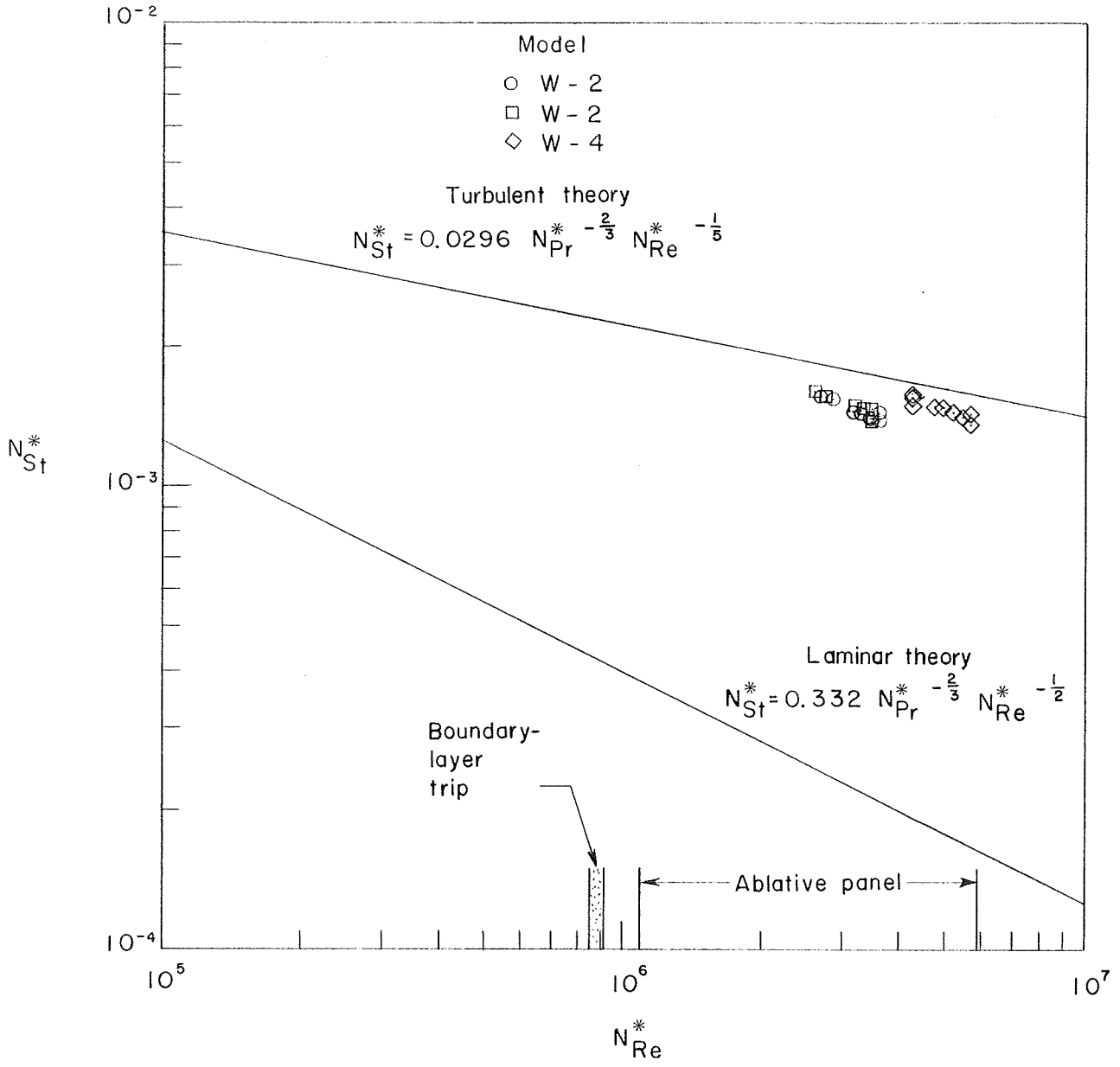


Figure 14.- Aerodynamic heating distribution on $30^0$ wedge insert plate with boundary-layer trip.

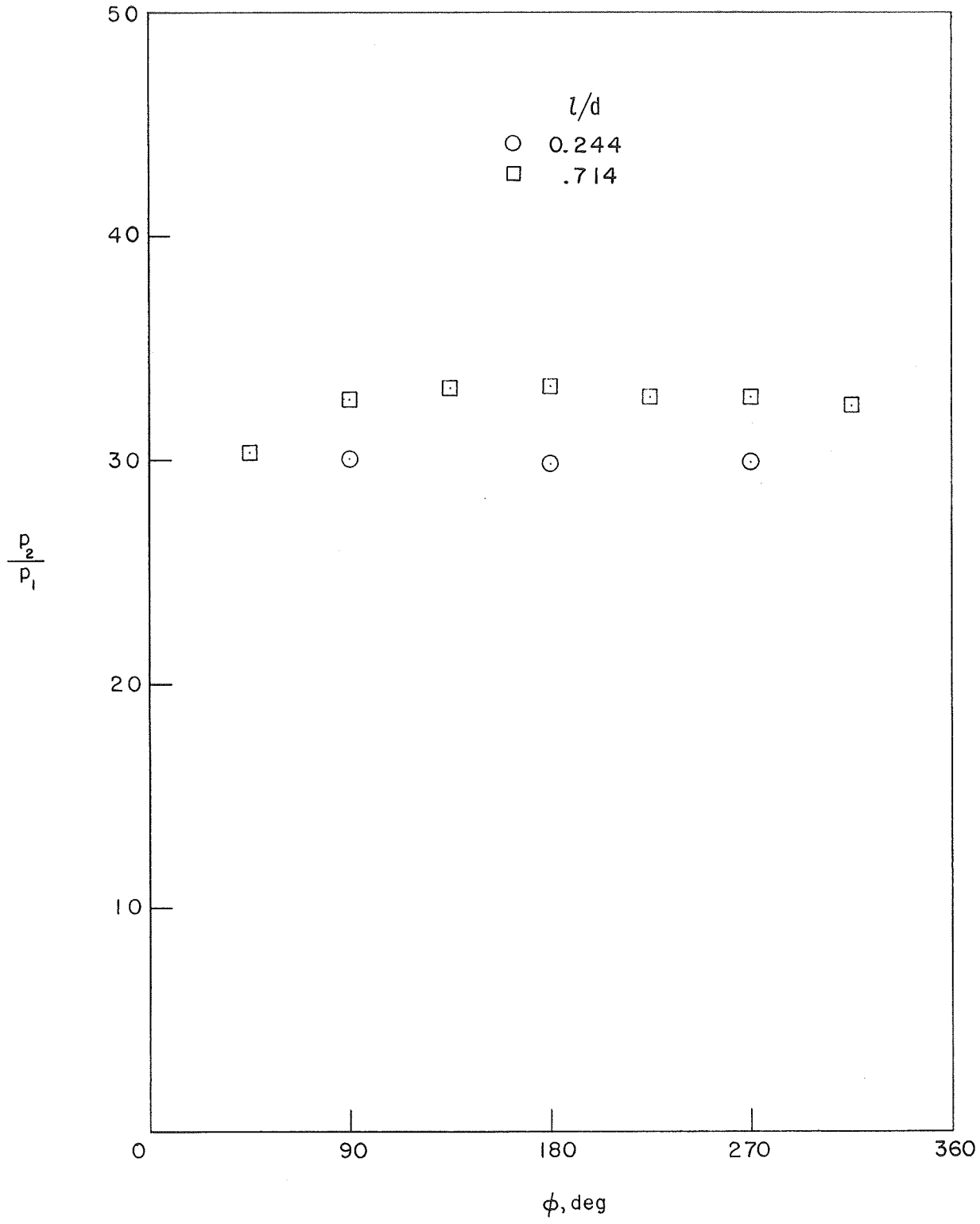


Figure 15.- Surface pressures on $36^0$ cone. $p_1 = 1.42$ kN/m$^2$.

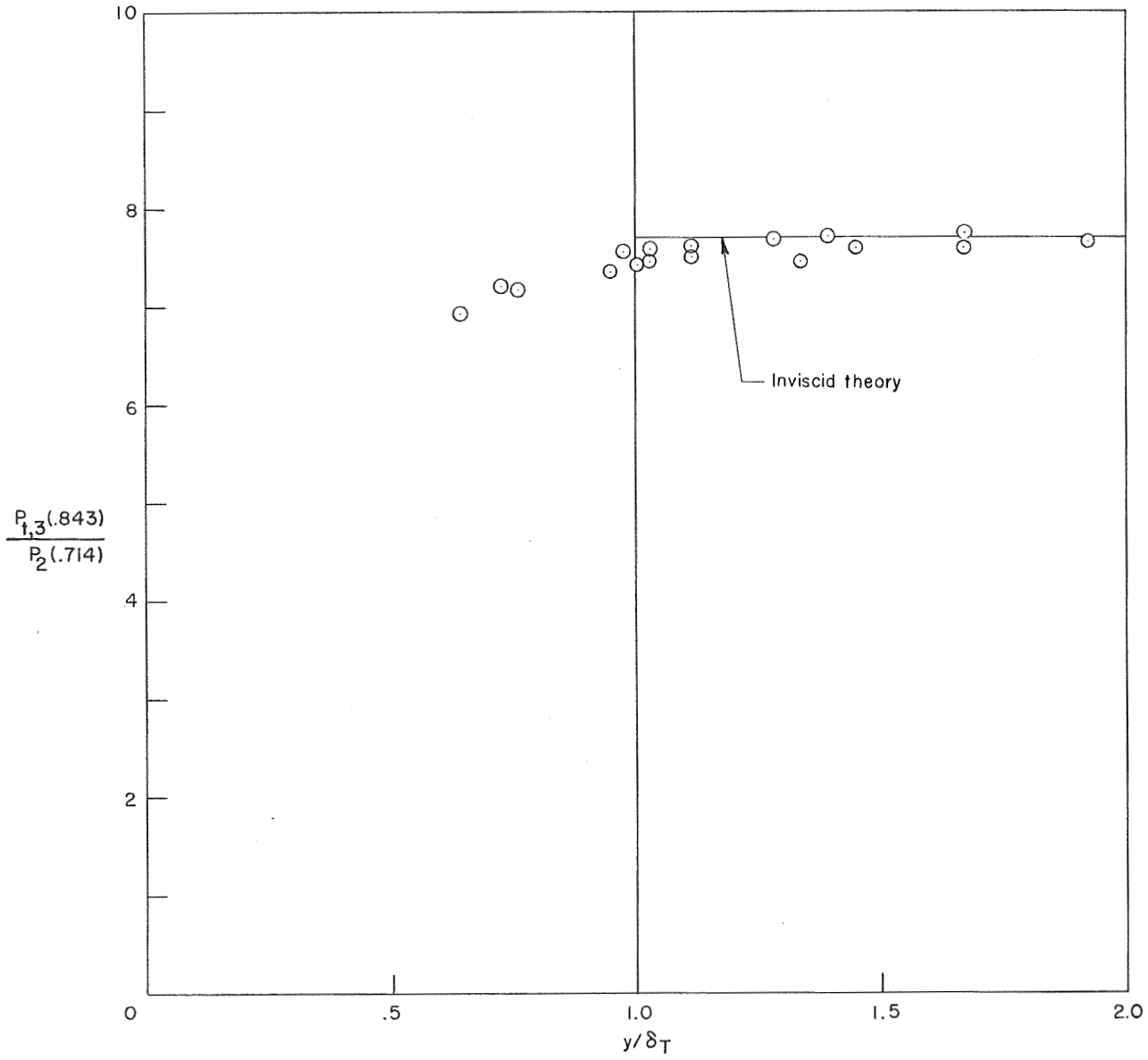


Figure 16.- Distribution of boundary-layer pitot pressure for $36^0$ cone. $l/d = 0.843$; $p_2 = 47.0\ kN/m^2$; $\delta_T = 4.6$ mm.

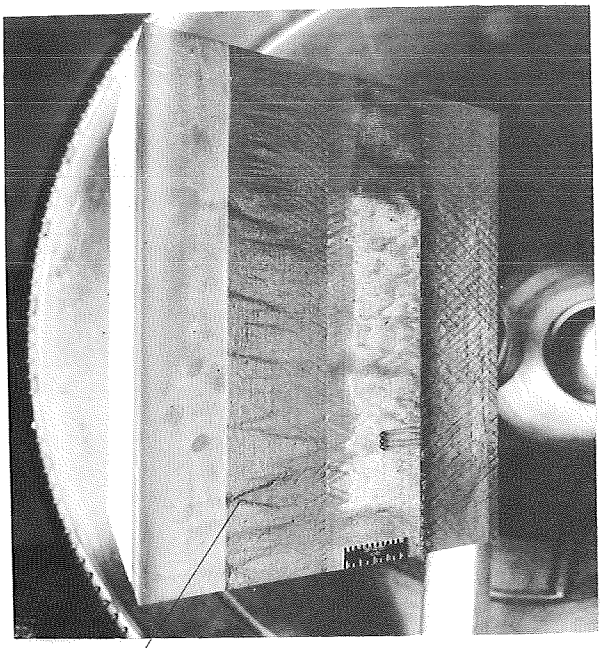


L-68-1831

(a) W-0; zones I and II.

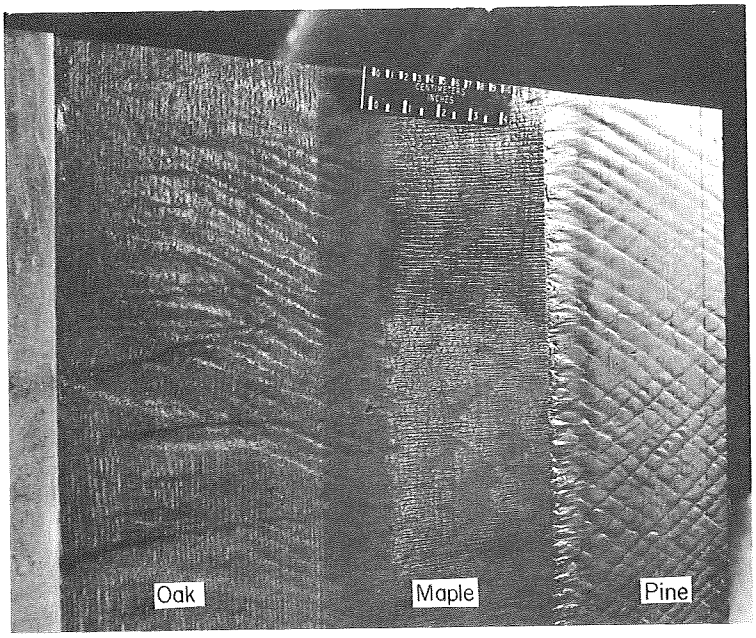


L-68-1837

(b) W-0; zone I.

Figure 17.- Groove patterns in wood panels.

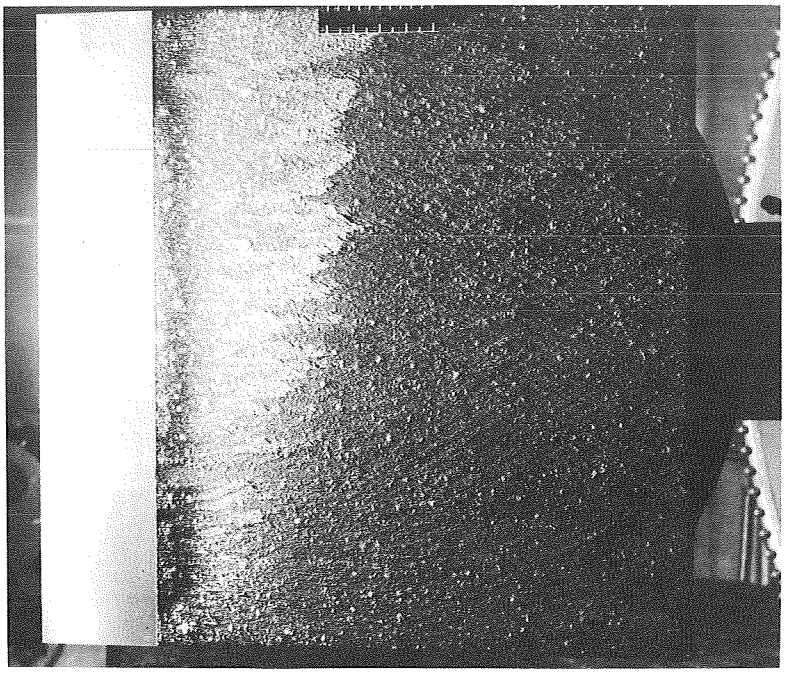

(a) W-1; zones III and IV. L-68-1913

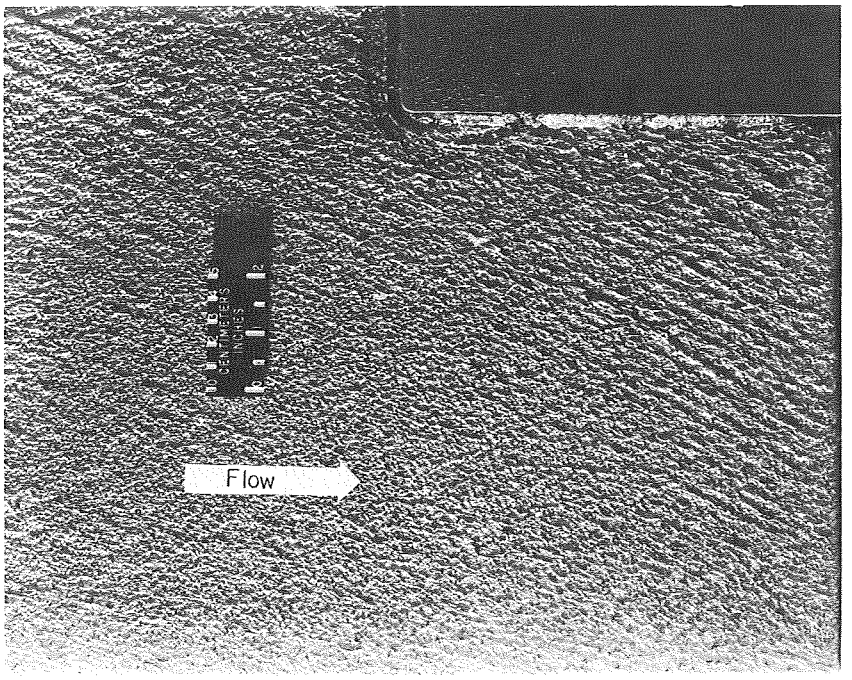


(b) W-4; zone II.

Figure 18.- Groove patterns in Lexan panels. L-68-4887

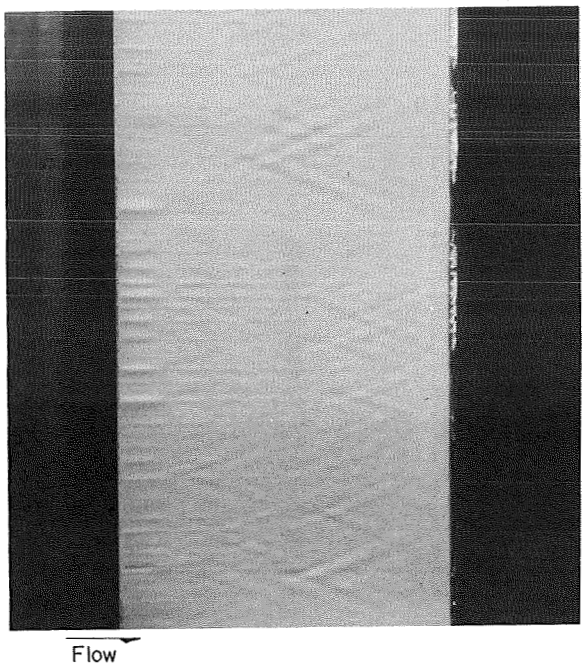


(a) W-2; zone II. L-68-3285

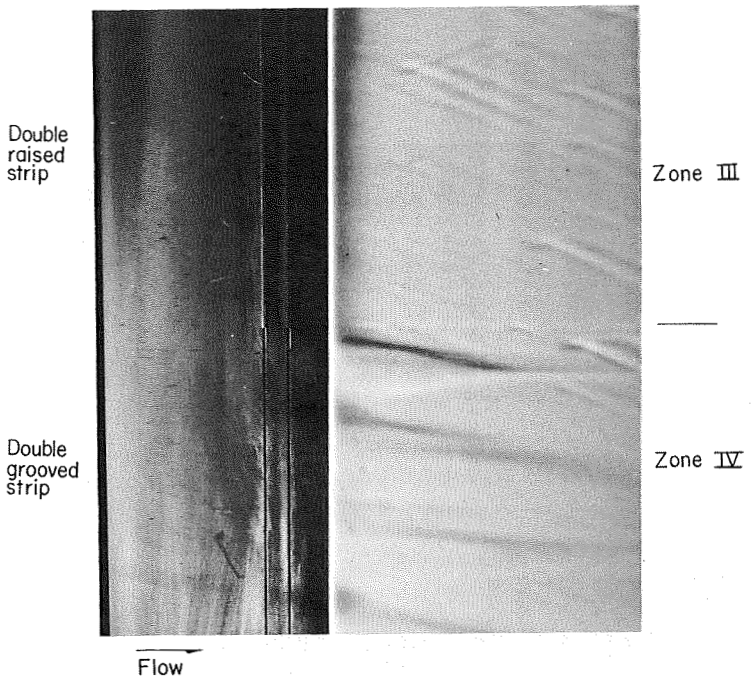


(b) W-2; zones III and IV. L-68-3775

Figure 19.- Groove patterns in teflon panels.

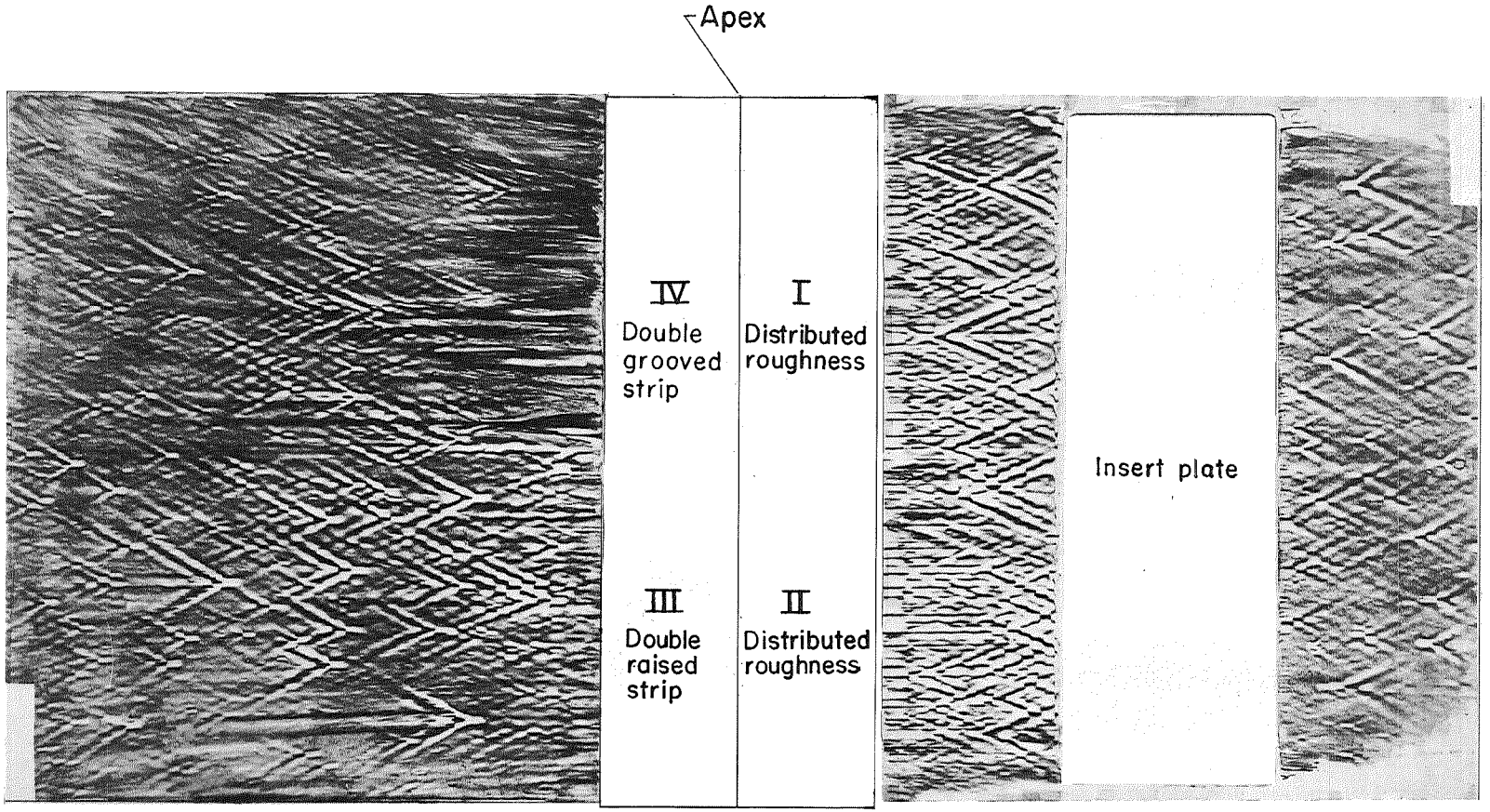


(a) W-2.

L-70-1571

Figure 20.- Developed surface tracings of wedge panels.

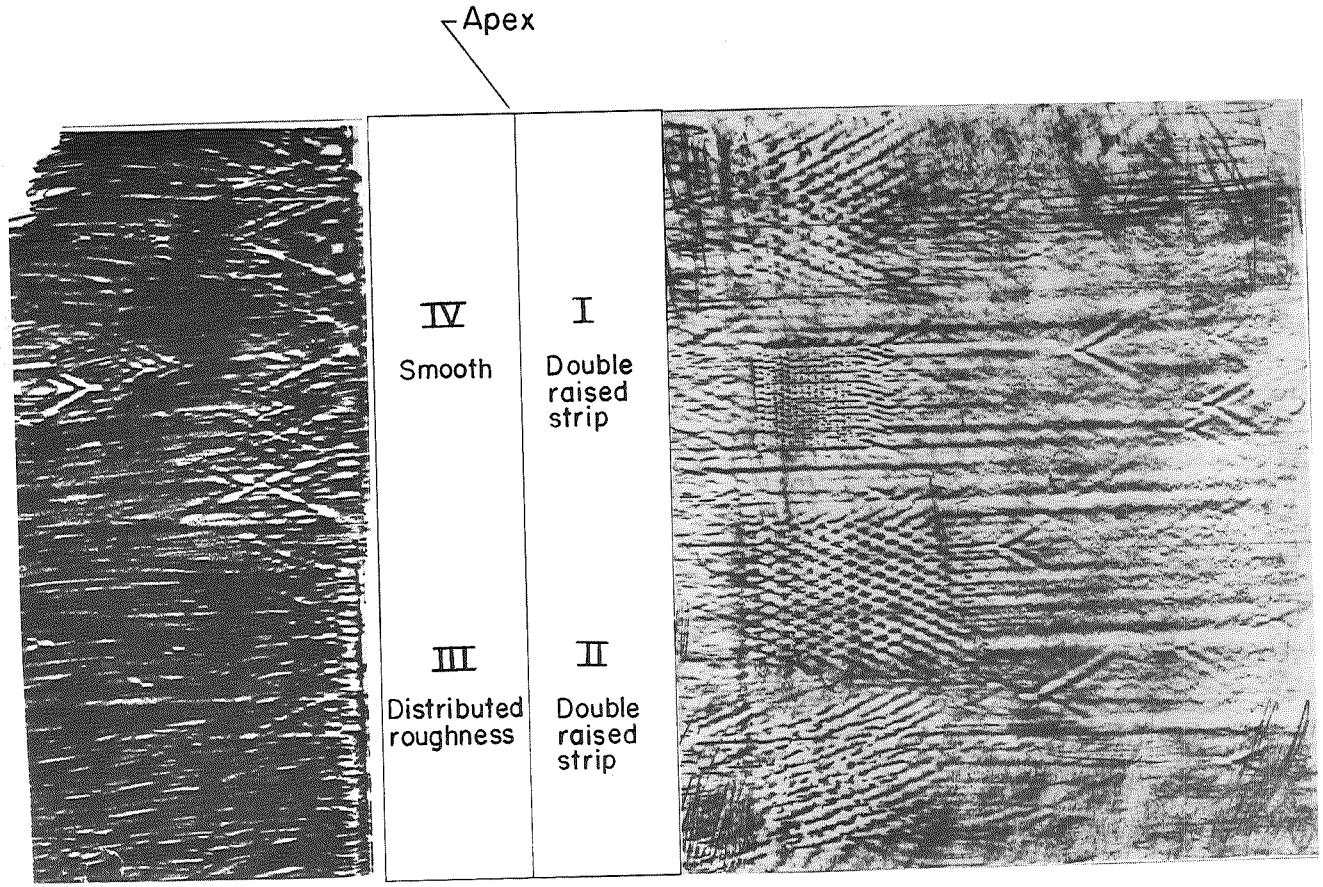


(b) W-3.

L-70-1572

Figure 20.- Continued.

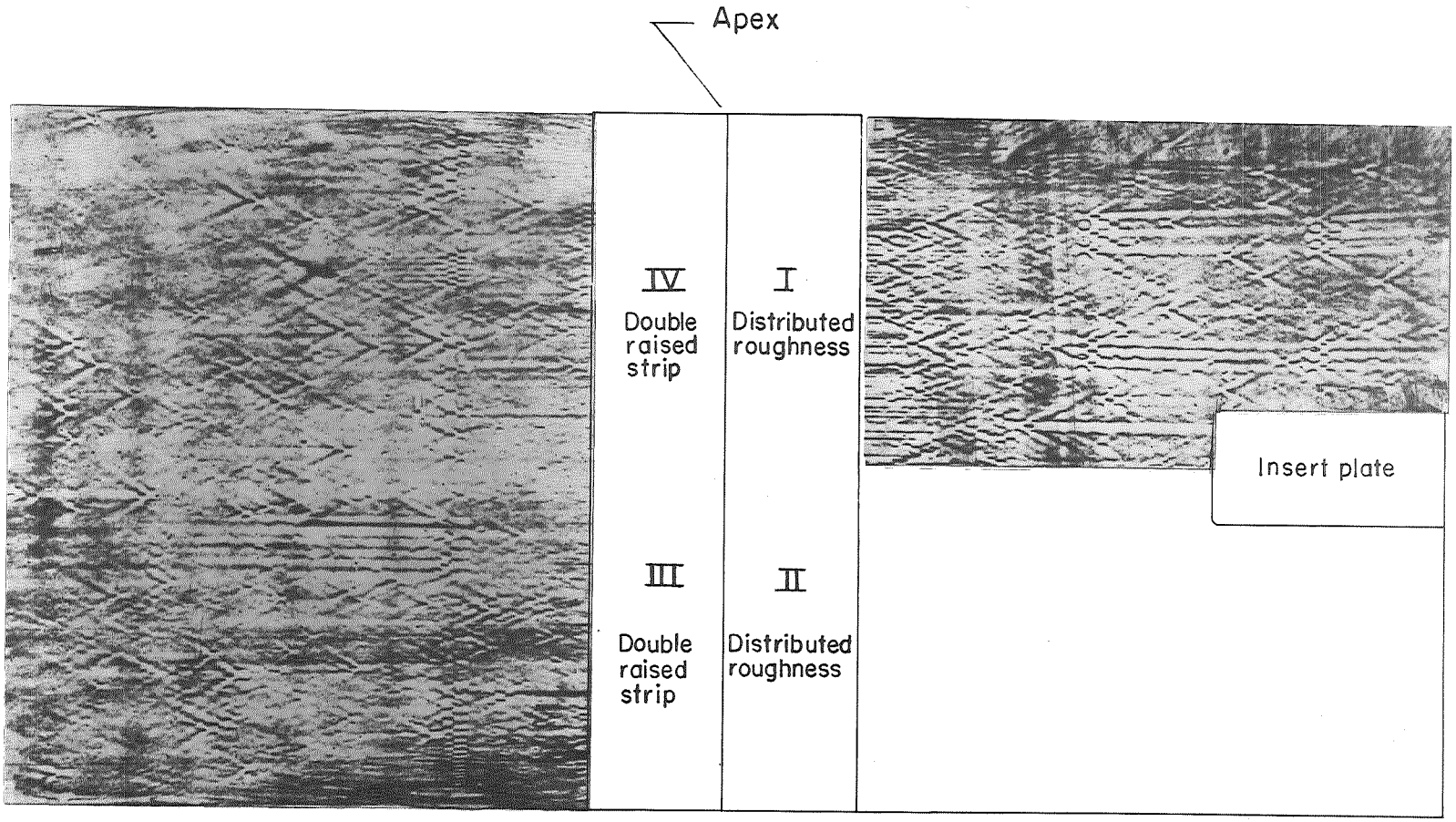


(c) W-4.

L-70-1573

Figure 20.- Concluded.

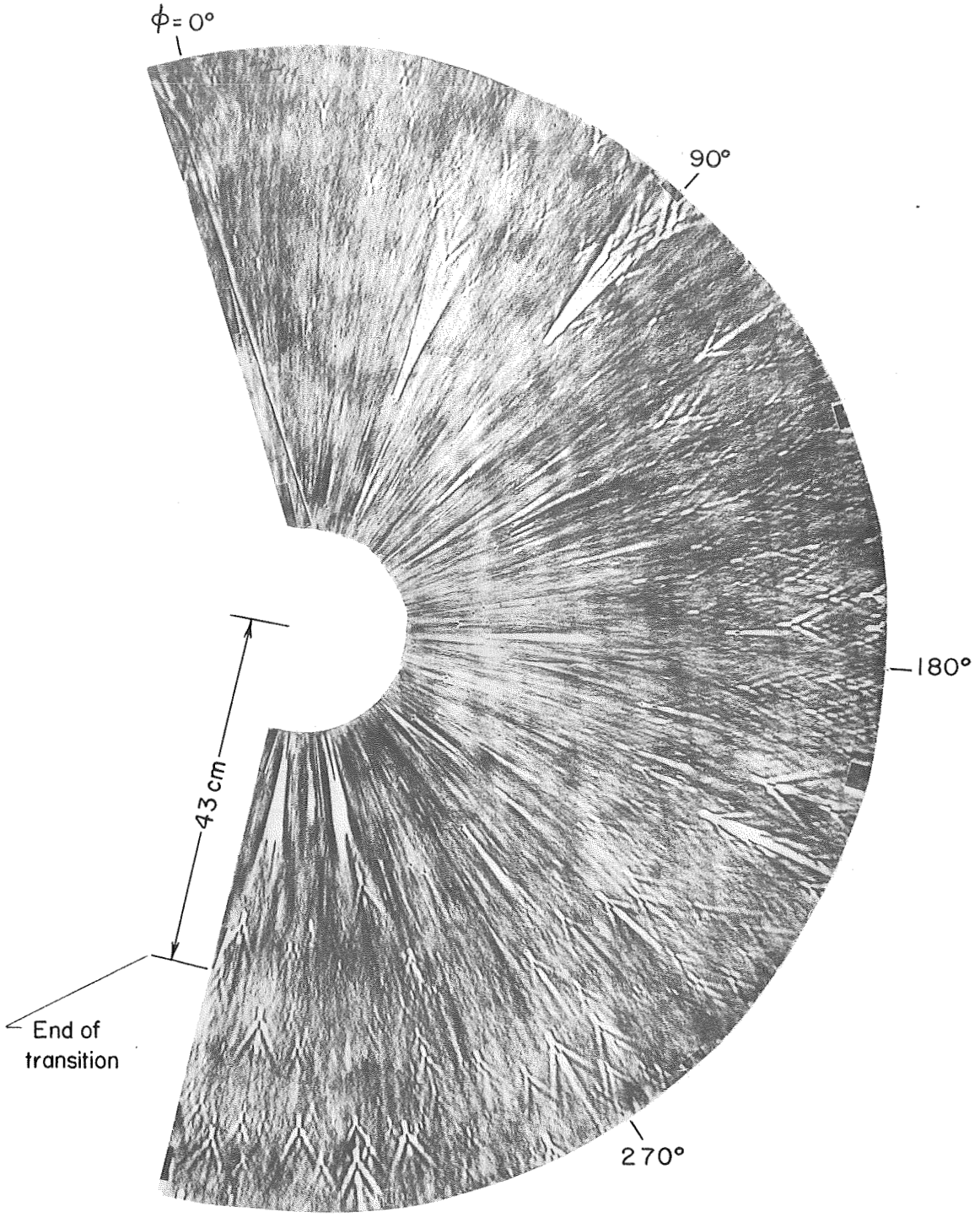


(a) C-1.

L-70-1574

Figure 21.- Developed surface tracings of cone frustum.

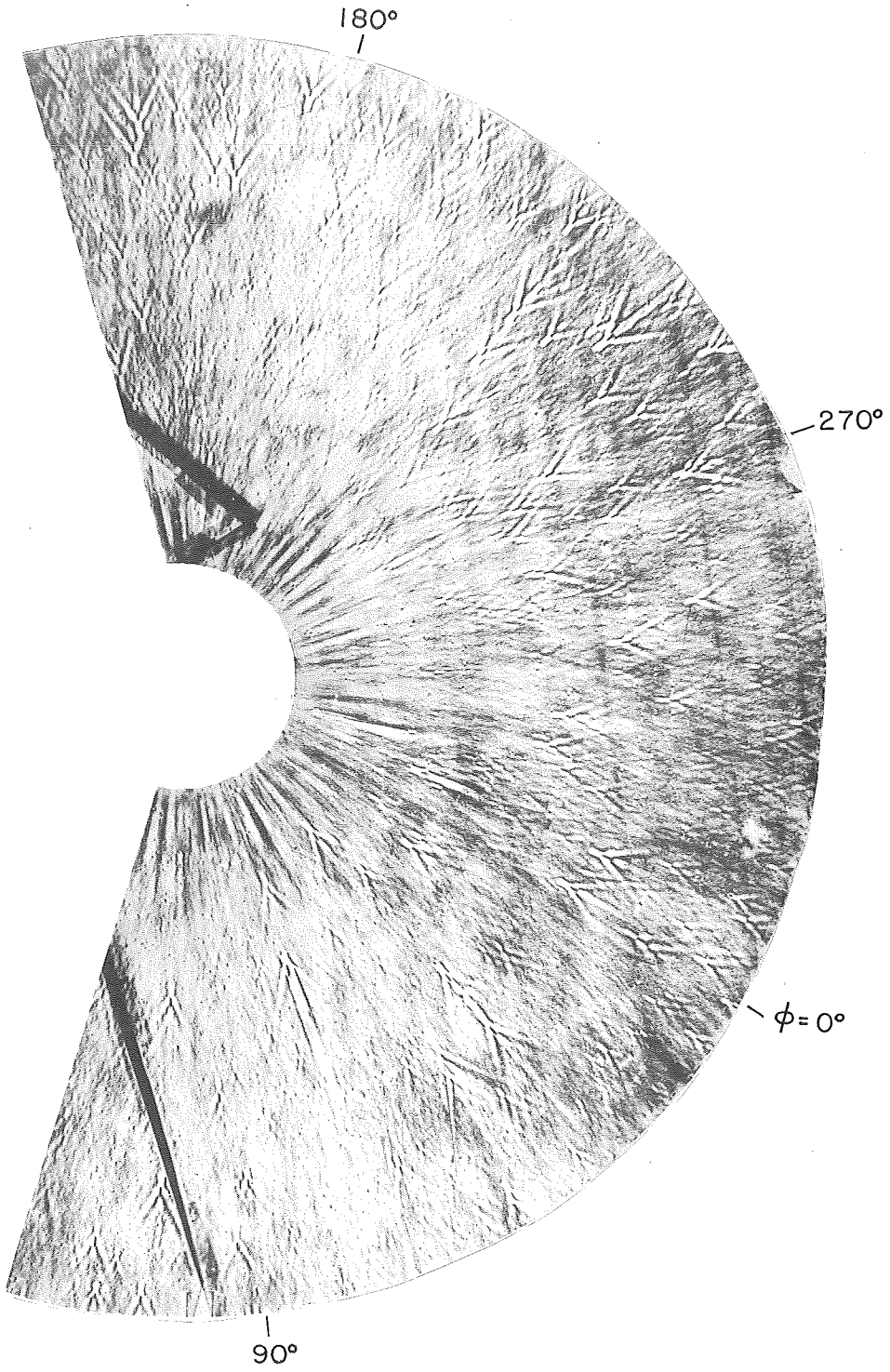


(b) C-2. L-70-1575

Figure 21.- Continued.

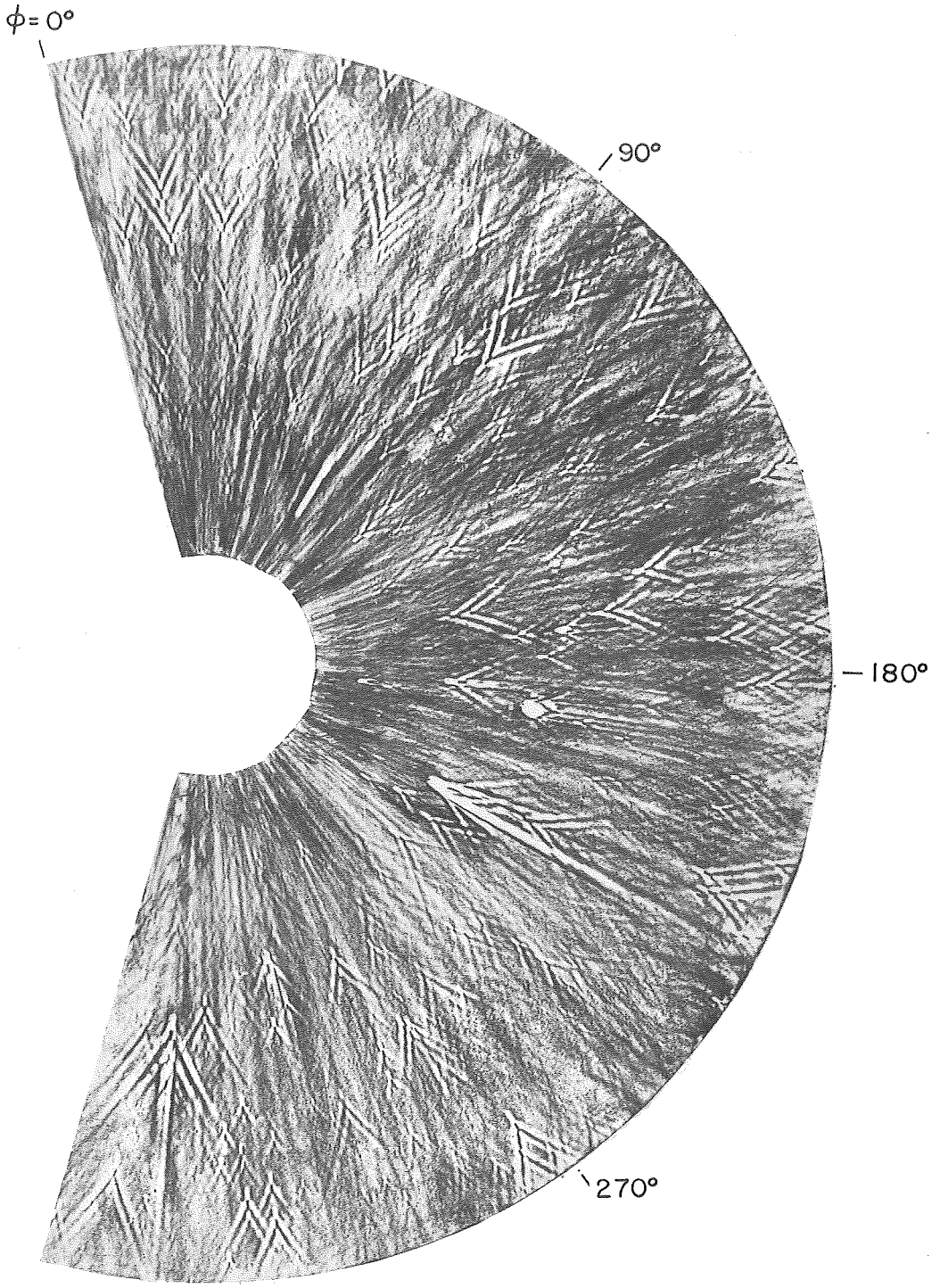


(c) C-3.

L-70-1576

Figure 21.- Continued.

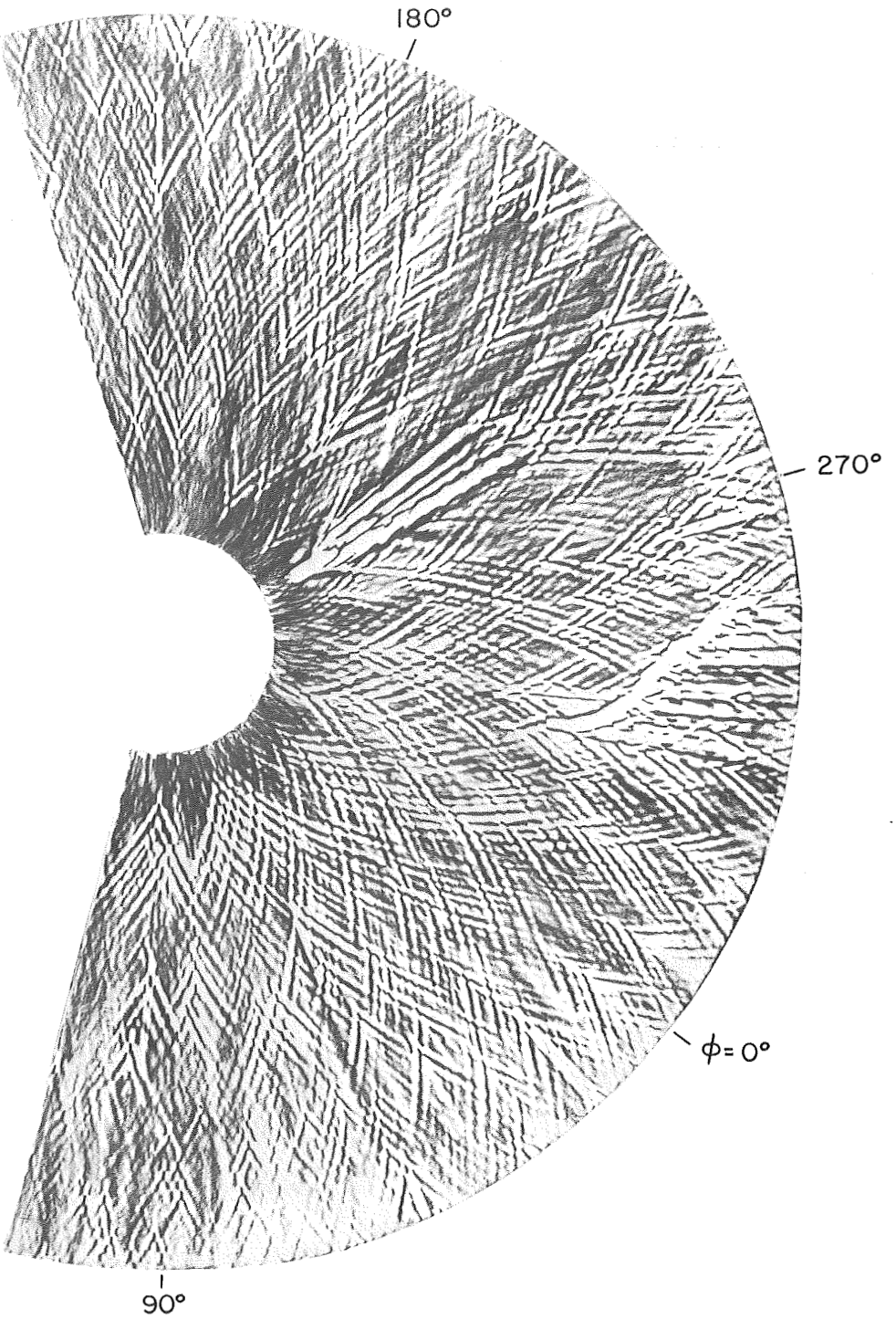


(d) C-4.

L-70-1577

Figure 21.- Continued.

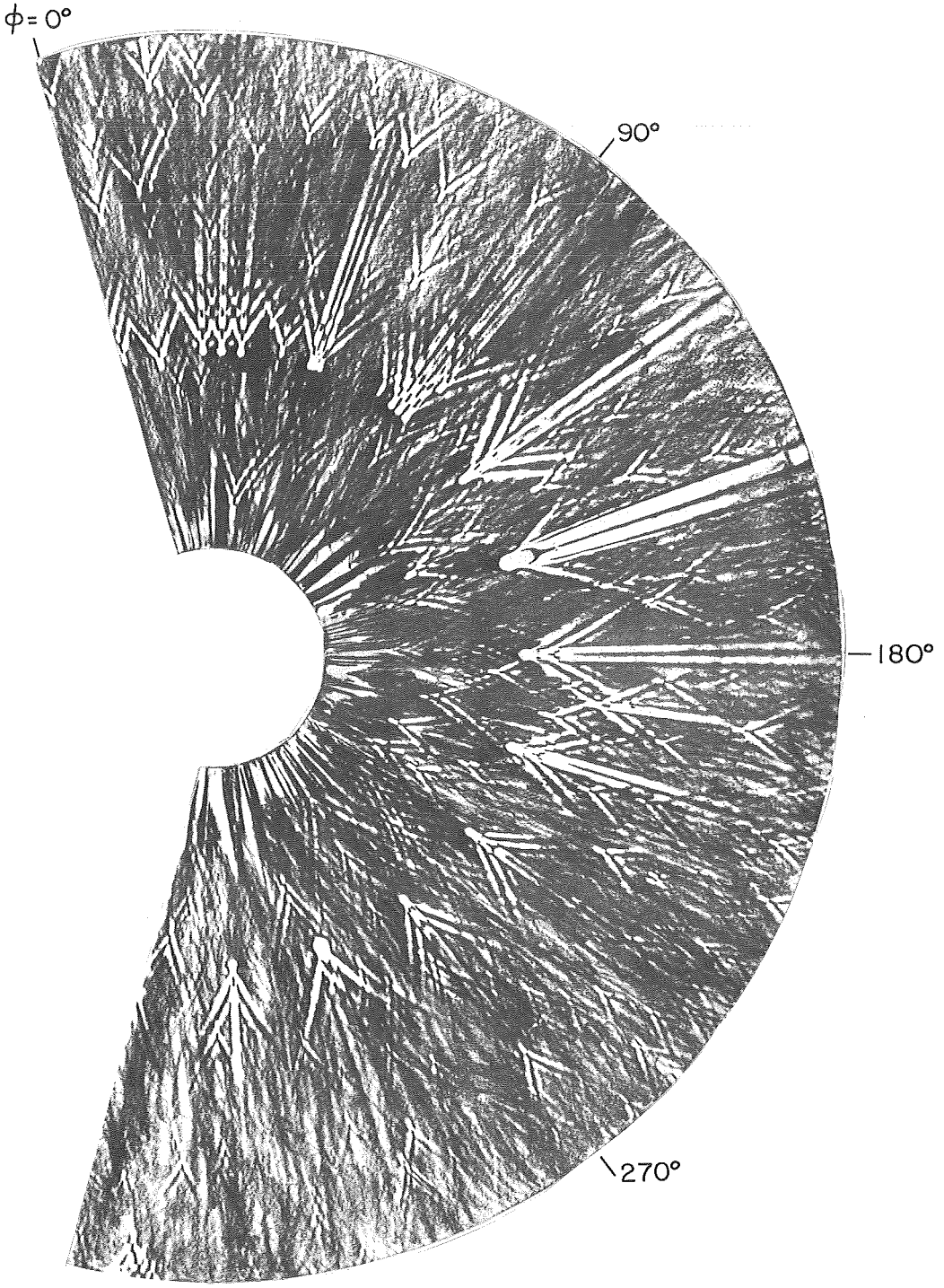


(e) C-5. L-70-1578

Figure 21.- Continued.

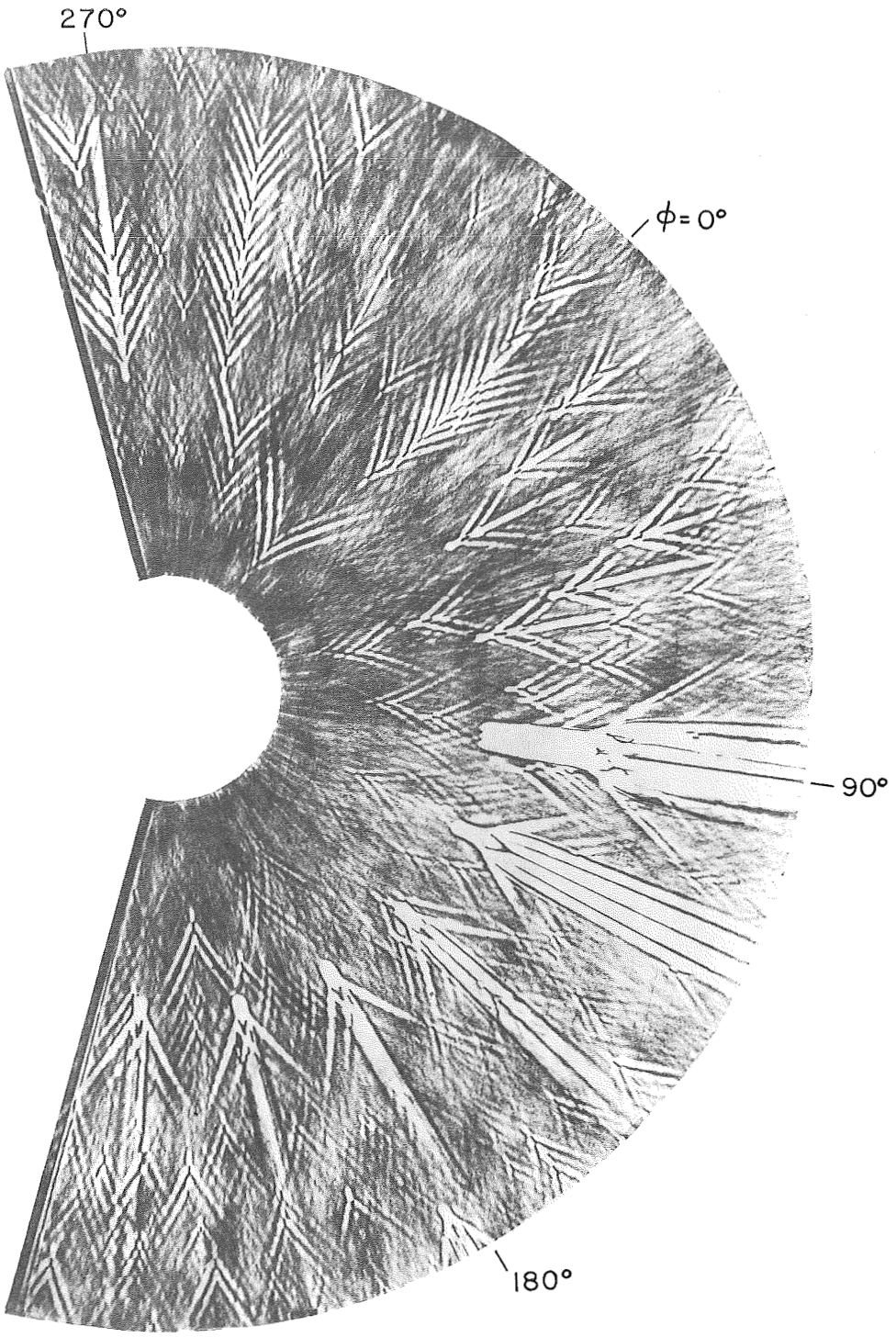


(f) C-6. L-70-1579

Figure 21.- Continued.

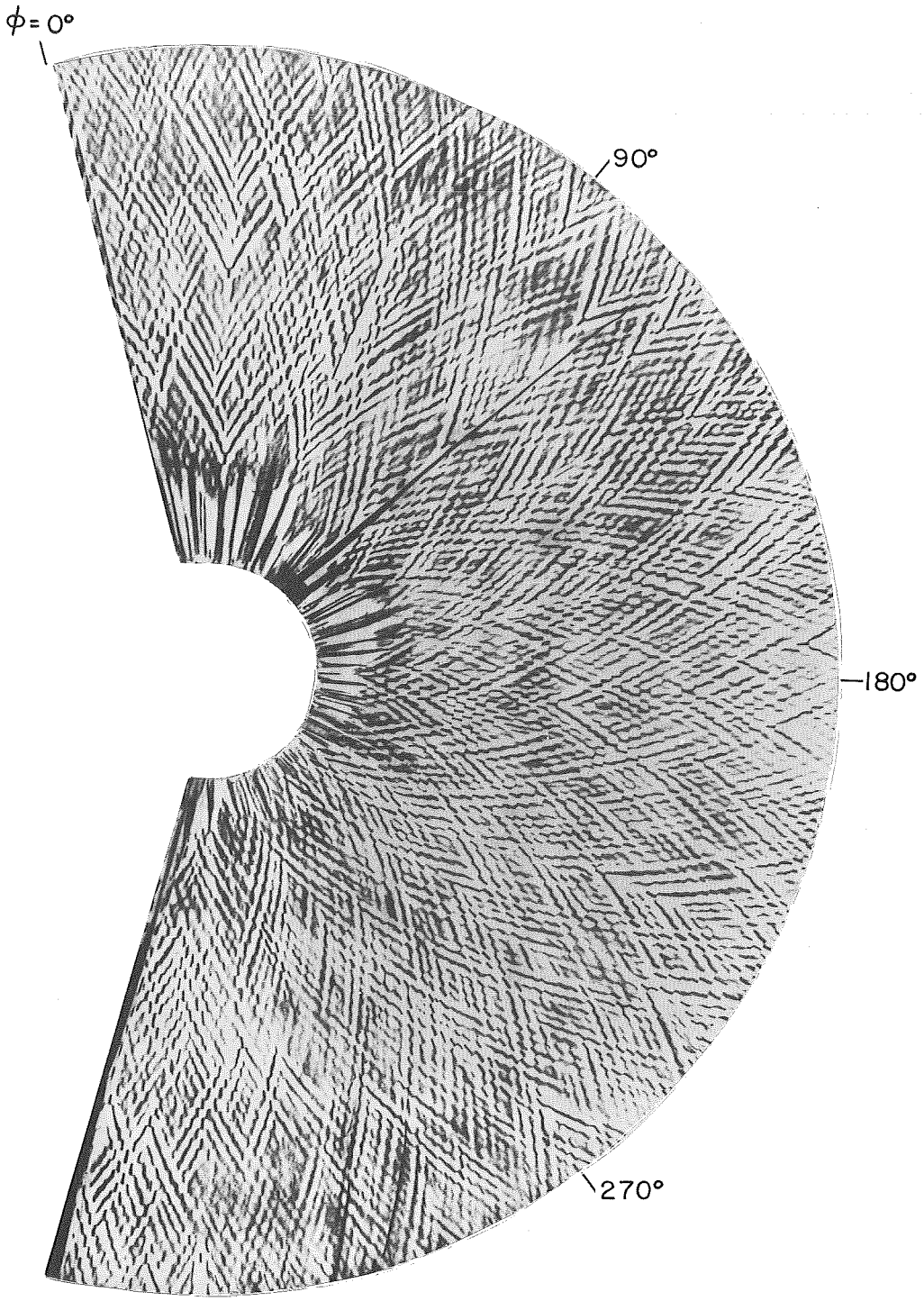


(g) C-7. L-70-1580

Figure 21.- Concluded.

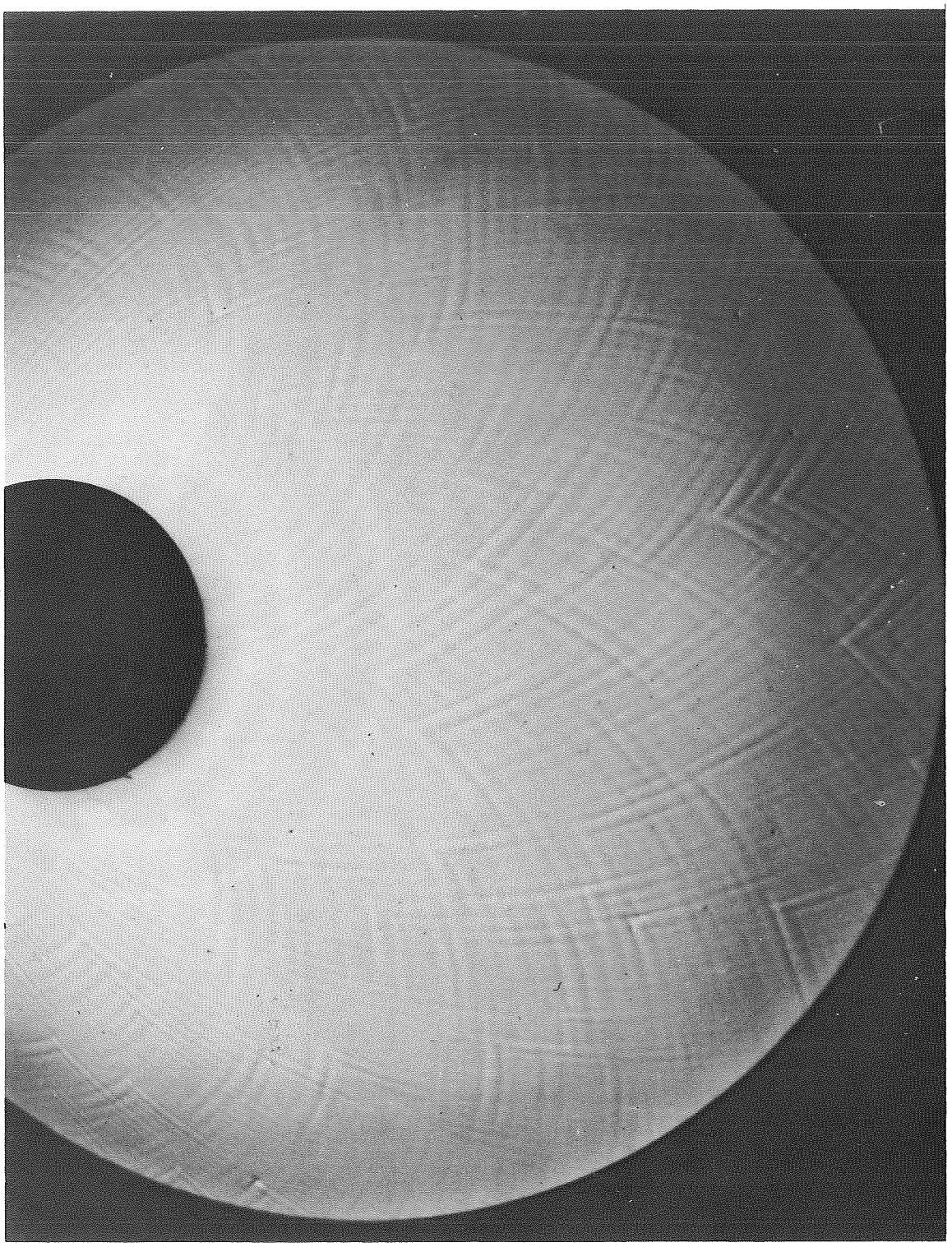

Figure 22.- Groove patterns in teflon cone C-7. L-68-5251

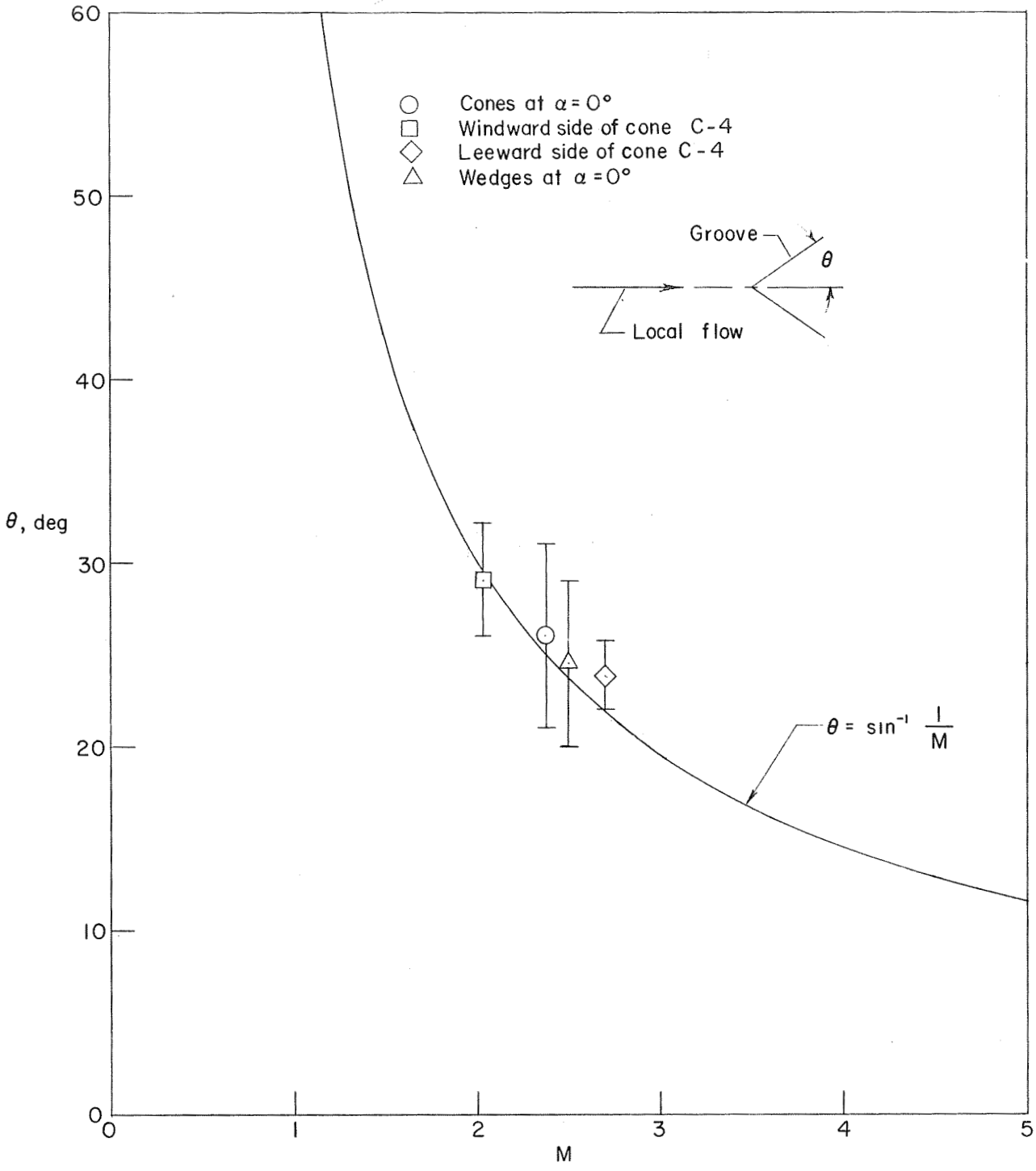


Figure 23.- Comparison of teflon cone and wedge groove angle with local Mach number.

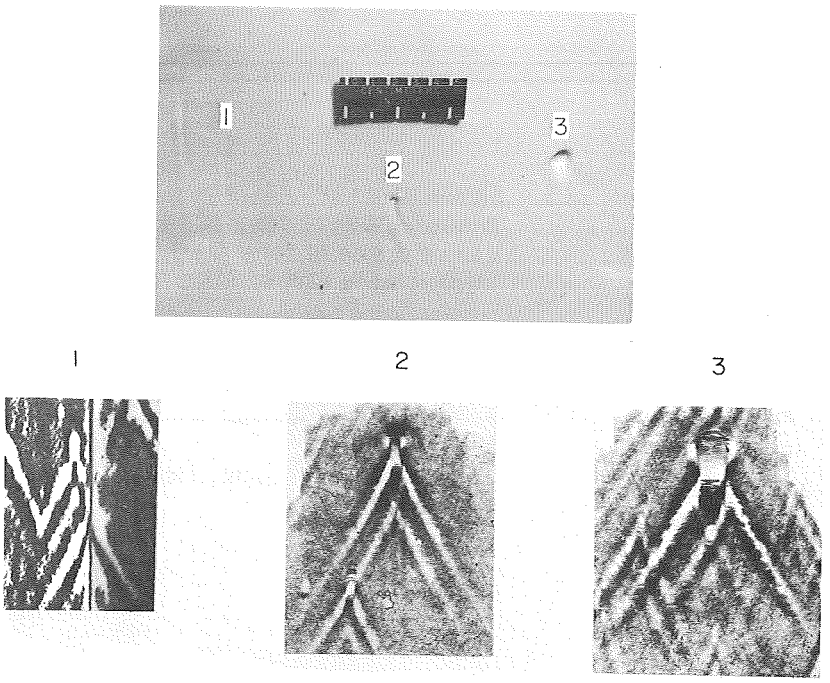


(a) C-5; disturbances 1, 2, and 3.

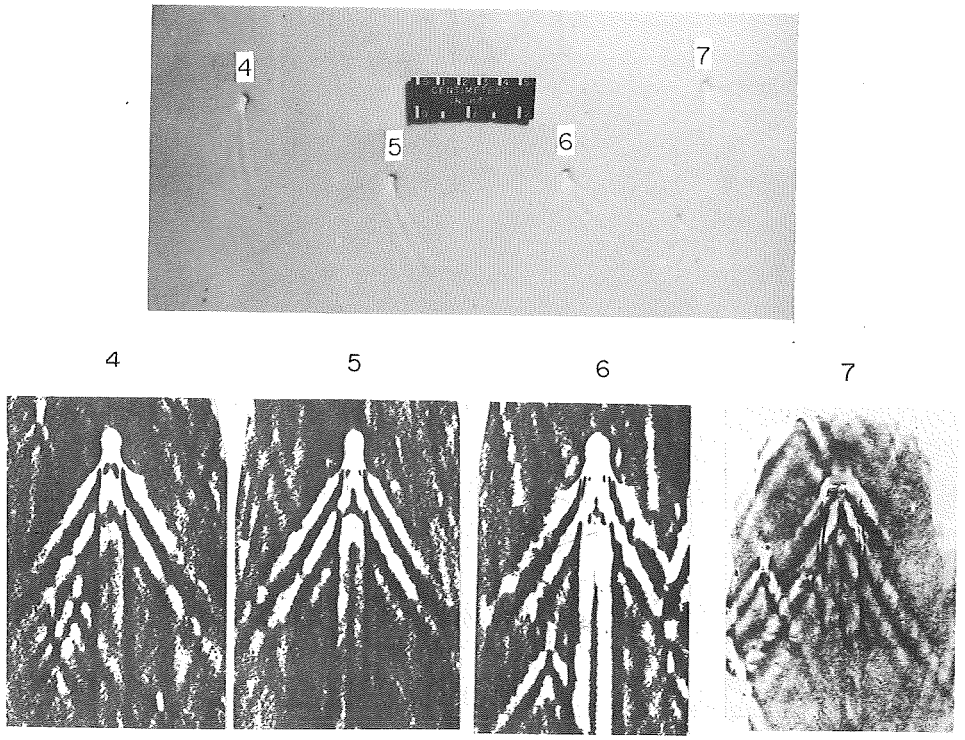


(b) C-5; disturbances 4, 5, 6, and 7.

Figure 24.- Photographs and tracings of disturbances on cone surfaces. L-70-1581

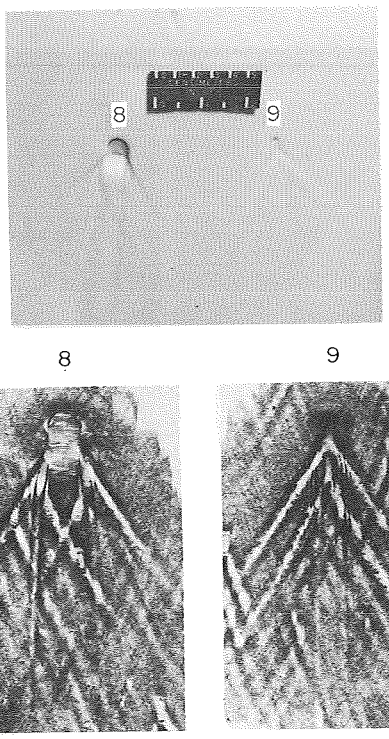


(c) C-5; disturbances 8 and 9.

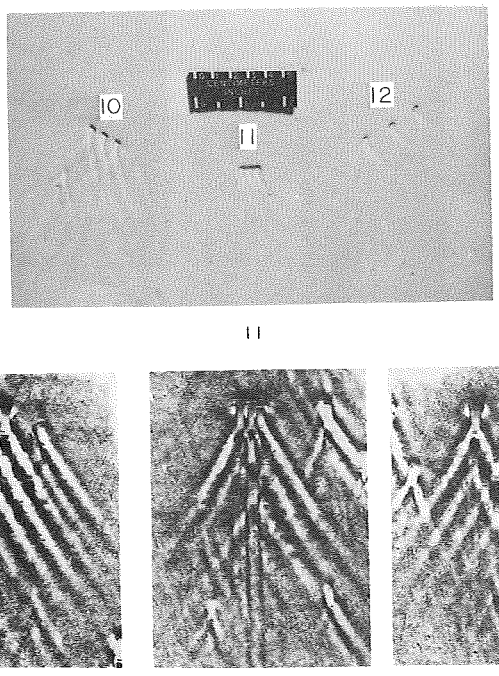


(d) C-5; disturbances 10, 11, and 12.

Figure 24.- Continued.

L-70-1582

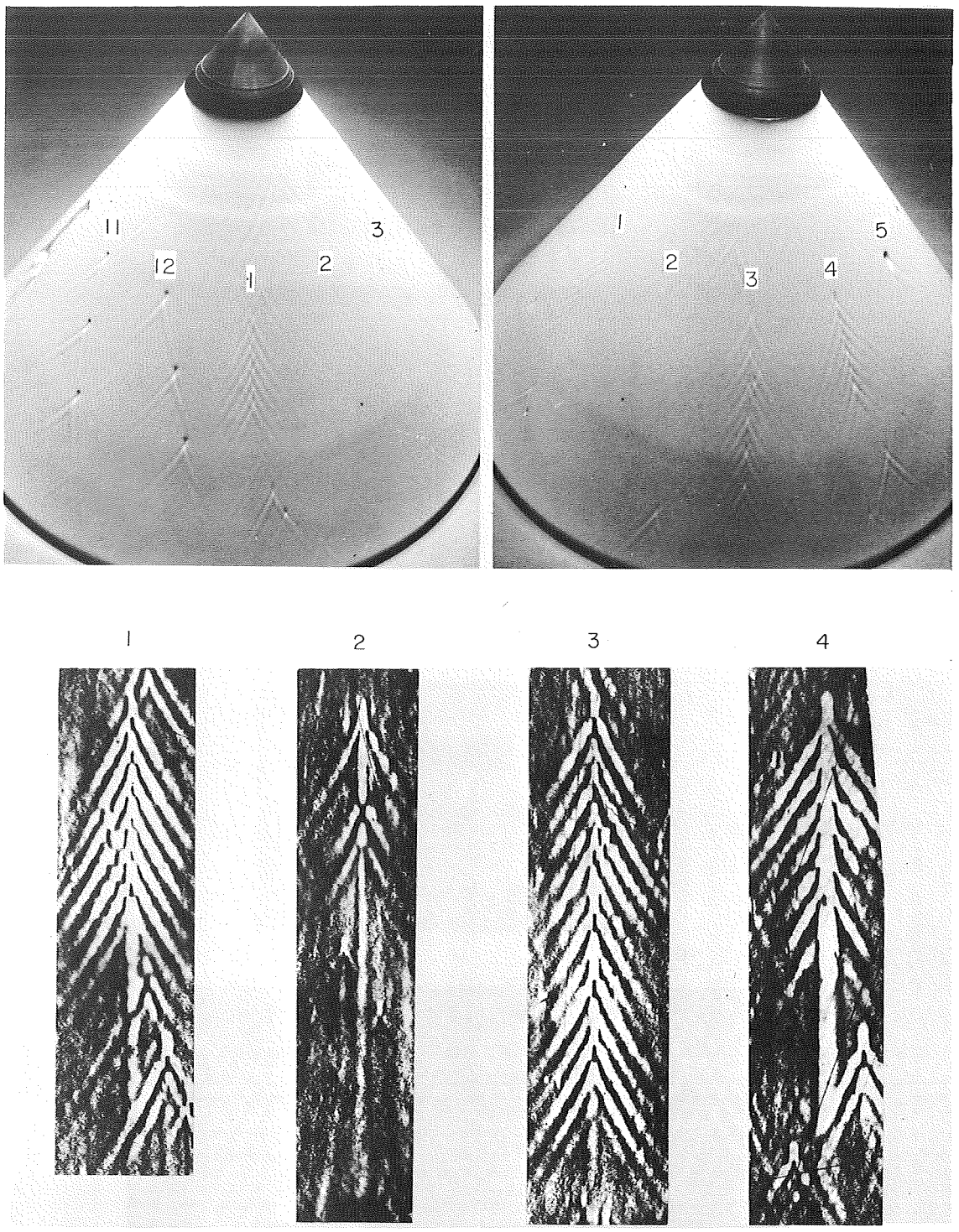


(e) C-6; disturbances 1, 2, 3, and 4.

Figure 24.- Continued.

L-70-1583

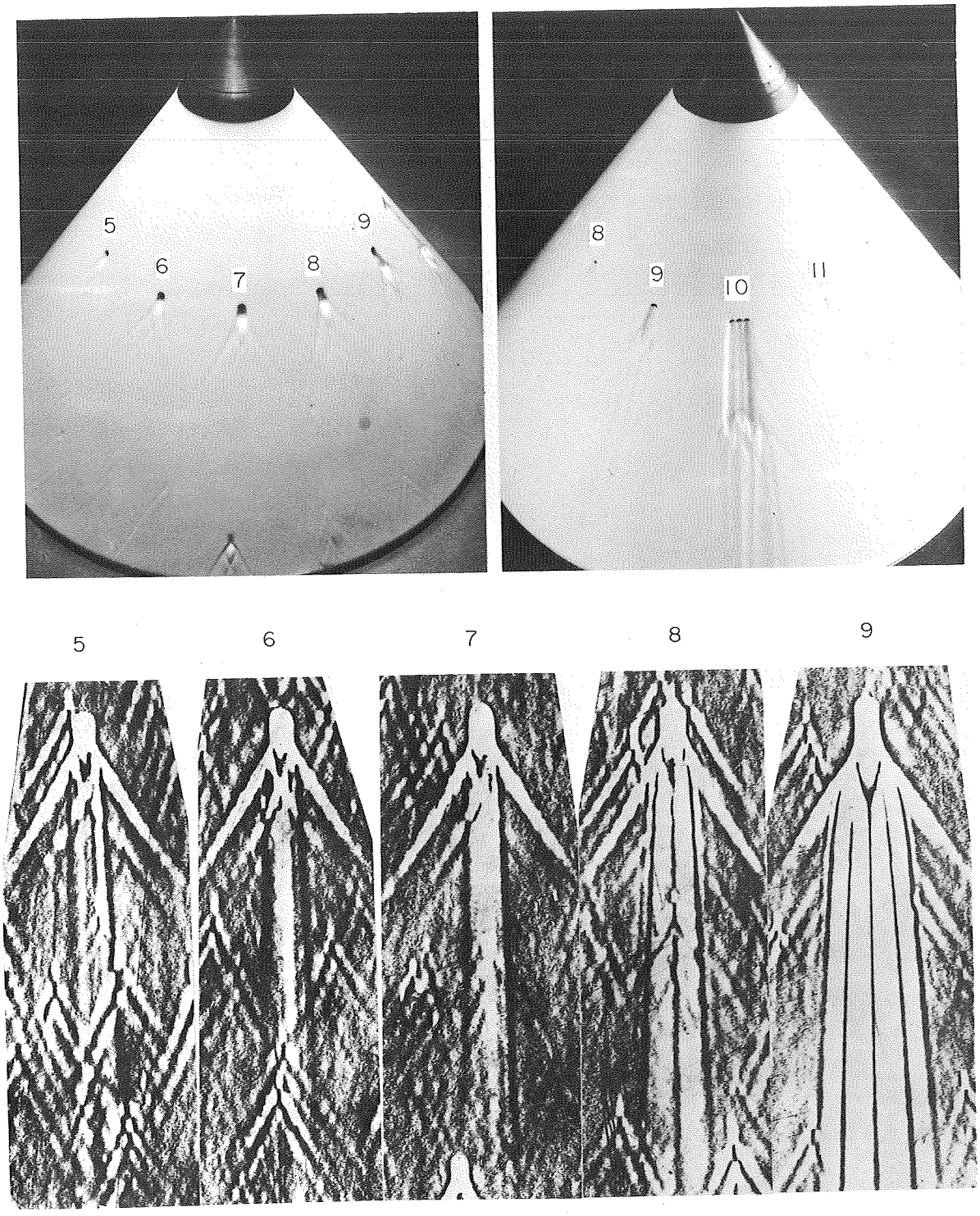


(f) C-6; disturbances 5, 6, 7, 8, and 9.

Figure 24.- Continued.

L-70-1584

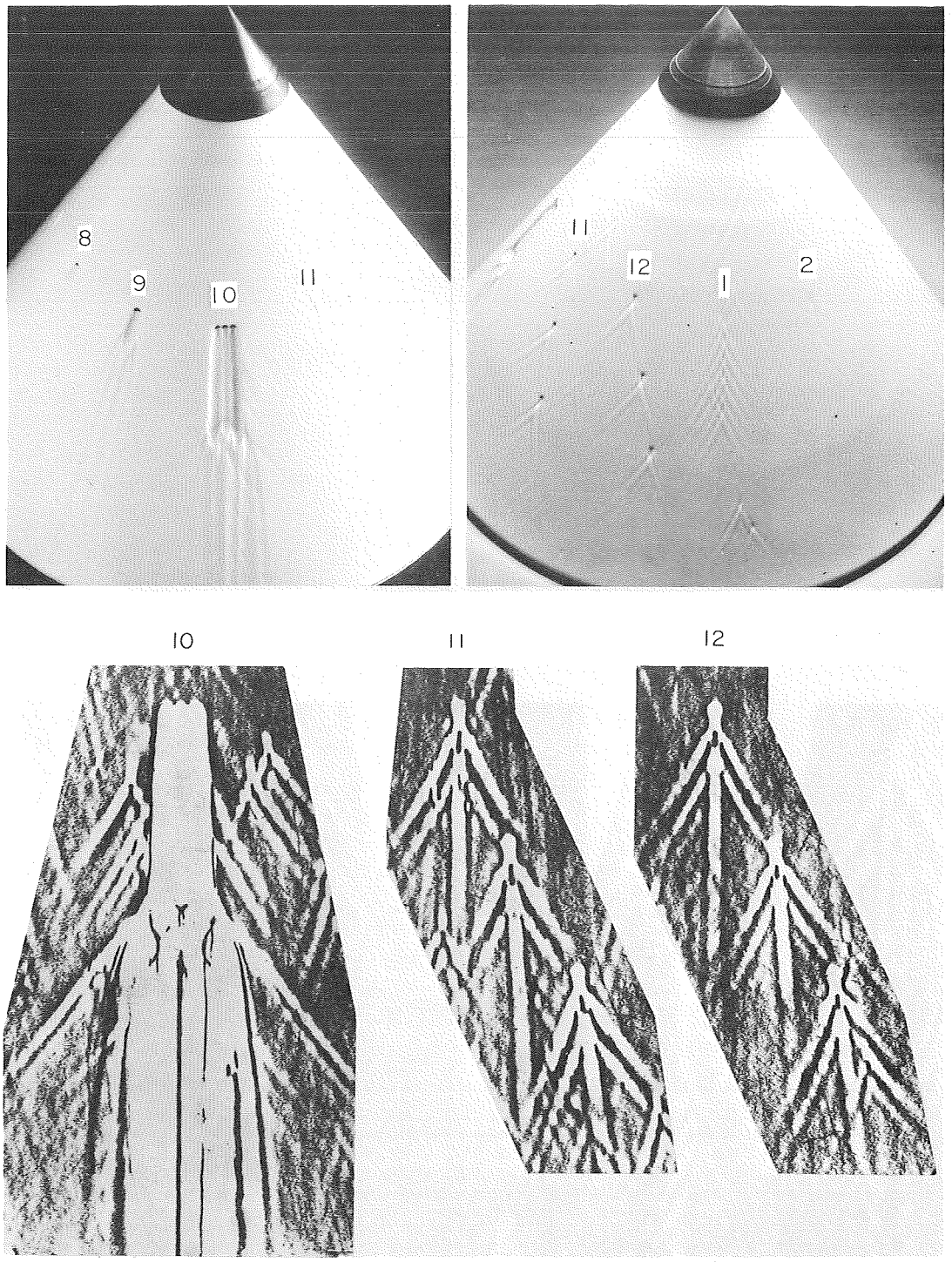


(g) C-6; disturbances 10, 11, and 12.

Figure 24.- Concluded. L-70-1585

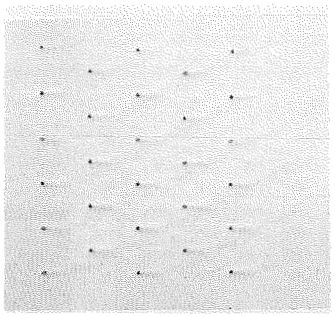

Disturbance 1

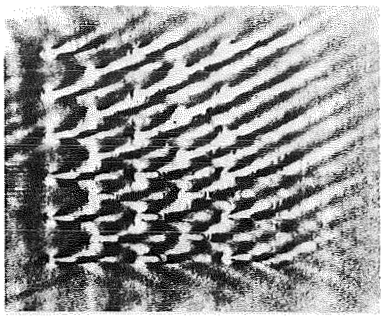

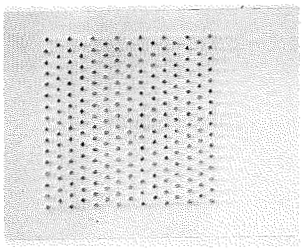

Disturbance 2

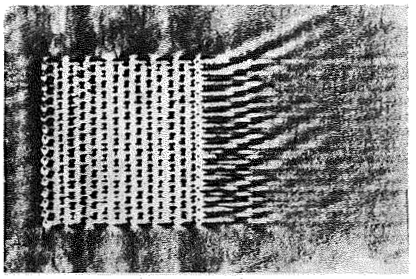

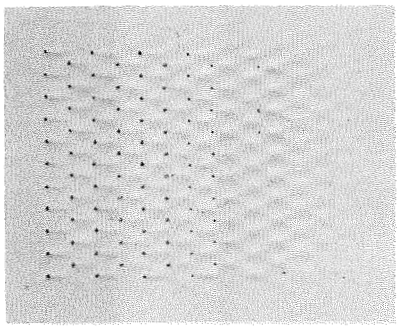

Disturbance 3

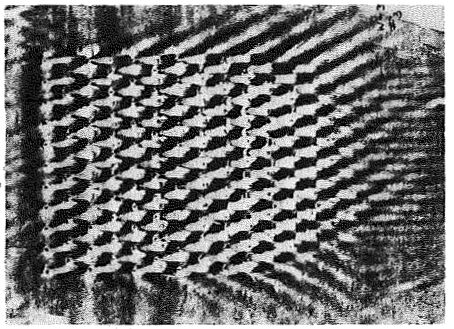

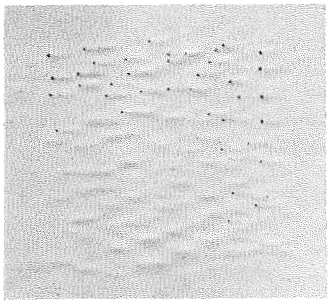

Disturbance 4

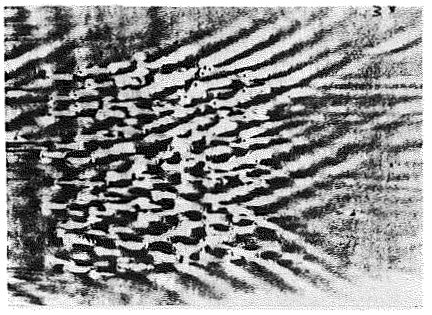

(a) W-3; zones I and II.

Figure 25.- Photographs and tracings of disturbances on wedge surfaces. L-70-1586

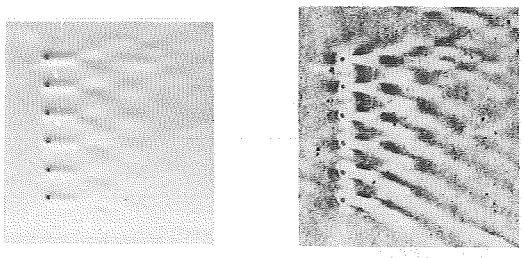

Disturbance 1

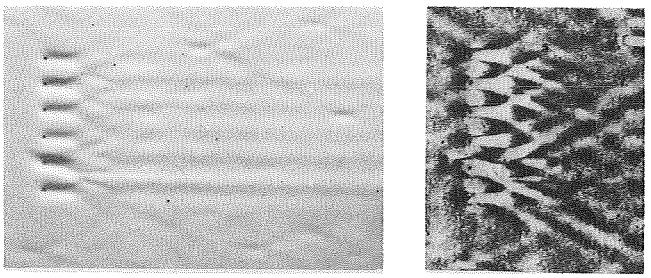

Disturbance 4

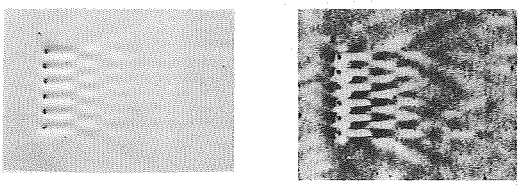

Disturbance 2

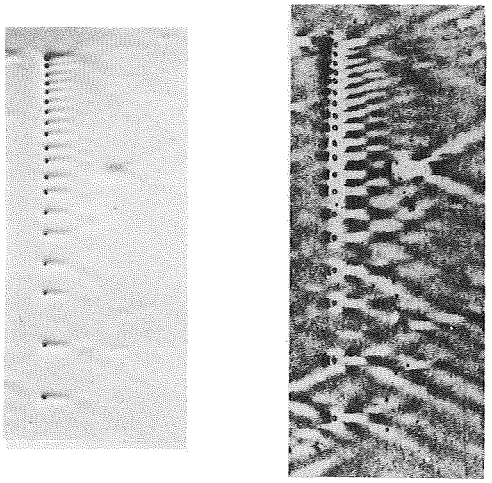

Disturbance 5

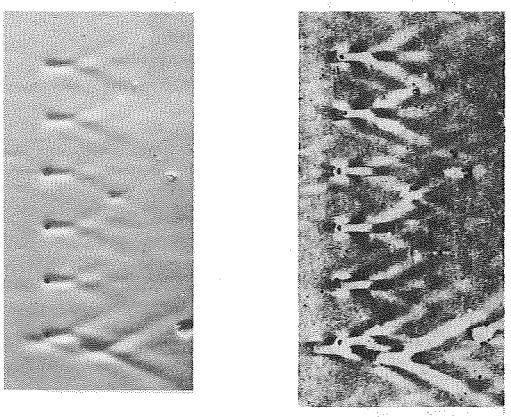

Disturbance 3

(b) W-4; zones III and IV.

Figure 25.- Continued.

L-70-1587

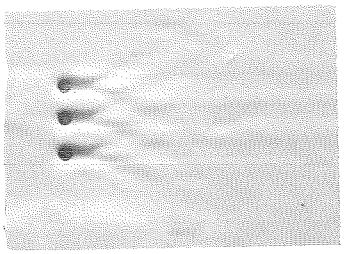

Disturbance 6

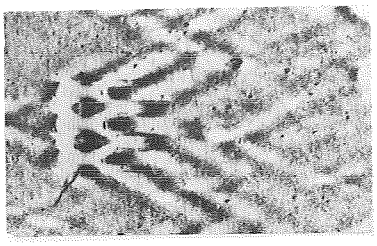

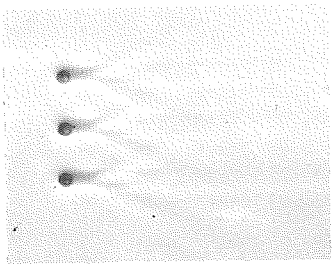

Disturbance 7

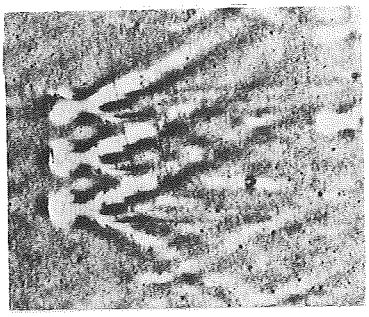

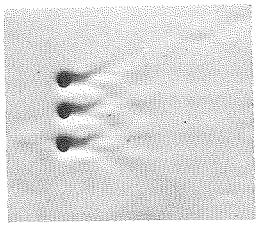

Disturbance 8

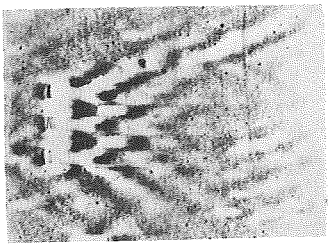

Disturbance 9

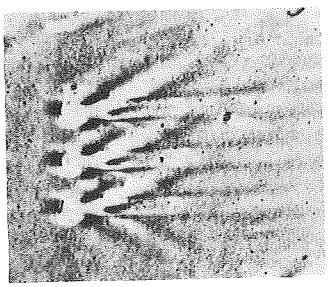

(c) W-4; zone I.

Figure 25.- Concluded.

L-70-1588



NASA-Langley, 1970 —— 33 L-6979

*"The aeronautical and space activities of the United States shall be conducted so as to contribute . . . to the expansion of human knowledge of phenomena in the atmosphere and space. The Administration shall provide for the widest practicable and appropriate dissemination of information concerning its activities and the results thereof."*

—NATIONAL AERONAUTICS AND SPACE ACT OF 1958

# NASA SCIENTIFIC AND TECHNICAL PUBLICATIONS

TECHNICAL REPORTS: Scientific and technical information considered important, complete, and a lasting contribution to existing knowledge.

TECHNICAL NOTES: Information less broad in scope but nevertheless of importance as a contribution to existing knowledge.

TECHNICAL MEMORANDUMS: Information receiving limited distribution because of preliminary data, security classification, or other reasons.

CONTRACTOR REPORTS: Scientific and technical information generated under a NASA contract or grant and considered an important contribution to existing knowledge.

TECHNICAL TRANSLATIONS: Information published in a foreign language considered to merit NASA distribution in English.

SPECIAL PUBLICATIONS: Information derived from or of value to NASA activities. Publications include conference proceedings, monographs, data compilations, handbooks, sourcebooks, and special bibliographies.

TECHNOLOGY UTILIZATION PUBLICATIONS: Information on technology used by NASA that may be of particular interest in commercial and other non-aerospace applications. Publications include Tech Briefs, Technology Utilization Reports and Notes, and Technology Surveys.

*Details on the availability of these publications may be obtained from:*

SCIENTIFIC AND TECHNICAL INFORMATION DIVISION

NATIONAL AERONAUTICS AND SPACE ADMINISTRATION

**Washington, D.C. 20546**